

<https://doi.org/10.1038/s41522-025-00698-7>

Multi-omics profiling of dairy cattle oxidative stress identifies hindgut-derived *Phascolarctobacterium succinatutens* exhibiting antioxidant activity

Check for updates

Duo Gao^{1,3}, Yimin Zhuang^{1,3}, Shuai Liu¹, Boyan Ma¹, Yiming Xu¹, Hongxing Zhang¹, Yiliyaer Nuermainaiti¹, Tianyu Chen¹, Guobin Hou¹, Wenli Guo¹, Jingtao You¹, Zhiyu Huang¹, Jianxin Xiao^{1,2}, Wei Wang¹, Mengmeng Li¹, Shengli Li¹ & Zhijun Cao¹ ✉

An imbalance between oxidative and antioxidant processes in the host can lead to excessive oxidation, a condition known as oxidative stress (OS). Although changes in the hindgut microbiota have been frequently linked to OS, the specific microbial and metabolic underpinnings of this association remain unclear. In this study, we enrolled 81 postpartum Holstein cows and stratified them into high oxidative stress (HOS, $n = 9$) and low oxidative stress (LOS, $n = 9$) groups based on the oxidative stress index (OSi). Using a multi-omics approach, we performed 16S rRNA gene sequencing to evaluate microbial diversity, conducted metagenomic analysis to identify functional bacteria, and utilized untargeted metabolomics to profile serum metabolites. Our analyses revealed elevated levels of kynurenine, formyl-5-hydroxykynurenine, and 5-hydroxyindole-3-acetic acid in LOS dairy cows. Additionally, the LOS cows had a higher abundance of short-chain fatty acids (SCFAs)-producing bacteria, including *Bacteroidetes bacterium*, *Paludibacter propionigenes*, and *Phascolarctobacterium succinatutens* (*P. succinatutens*), which were negatively correlated with OSi. To explore the potential role of these bacteria in mitigating OS, we administered *P. succinatutens* (10^8 cfu/day for 14 days) to C57BL/6 J mice ($n = 10$). Oral administration of *P. succinatutens* significantly increased serum total antioxidant capacity, decreased total oxidants, and reduced OSi in mice. Moreover, this treatment promoted activation of the Nrf2-Keap1 antioxidant pathway, significantly enhancing the enzymatic activities of GSH-Px and SOD, as well as the concentrations of acetate and propionate in the colon. In conclusion, our findings suggest that systemic tryptophan metabolism and disordered SCFAs production are concurrent factors influenced by hindgut microbiota and associated with OS development. Modulating the hindgut microbiota, particularly by introducing specific SCFAs-producing bacteria, could be a promising strategy for combating OS.

Oxidative stress (OS) is a hallmark of numerous human diseases and has been implicated in over 100 pathological conditions, including obesity, diabetes, liver disease, and gastrointestinal disorders^{1–4}. Various factors, including lifestyle, metabolic disturbances, inflammatory responses, and environmental influences, can intensify OS during the critical peripartum

period^{5–8}. Given its pervasive impact, OS should be acknowledged as the primary driver of many diseases as well as a product of intricate interrelated processes that warrant extensive investigation. Dairy cows are essential food-producing animals that have attracted significant research interest in recent years, particularly in the fields of nutrition, genetics, and health

¹State Key Laboratory of Animal Nutrition and Feeding, International Calf and Heifer Organization, College of Animal Science and Technology, China Agricultural University, Beijing, China. ²Animal Nutrition Institute, Sichuan Agricultural University, Chengdu, China. ³These authors contributed equally: Duo Gao, Yimin Zhuang. ✉ e-mail: caozhijun@cau.edu.cn

management^{9–11}. However, only a few studies have examined dairy cows as an OS model. Driven by elevated lactation demands, a grain-heavy diet, and intensive management practices, dairy cows experience substantial metabolic stress during the postpartum period, making them more susceptible to OS. In dairy cows, OS manifests prominently during the peripartum period due to metabolic adaptations required for lactation, including elevated lipolysis, hepatic ketogenesis, and mitochondrial oxidative phosphorylation. Clinically, OS in cows correlates with reduced lactation efficiency, heightened susceptibility to mastitis, metritis, and fatty liver, underscoring its detrimental impact on productivity and welfare^{12–14}. Additionally, dairy cows possess physiological characteristics similar to those of humans, including a gestational length of approximately 280 days, parity, and a high prevalence of singleton pregnancies¹⁵. Given these similarities, dairy cows offer a distinctive platform for exploring the mechanisms underlying OS, which could potentially yield valuable insights beneficial to both veterinary and human health.

Under normal conditions, the antioxidant system maintains the redox balance of cells by counteracting the accumulation of reactive oxygen and nitrogen species (RONS) generated during metabolic stress. OS is defined as an imbalance between the production of oxidants and the host's antioxidant defenses, leading to oxidative damage of lipids, proteins, and DNA. This molecular damage disrupts cellular homeostasis, impairing critical physiological processes such as mitochondrial energy production, immune function, and nutrient metabolism. For instance, lipid peroxidation generates malondialdehyde (MDA), while protein carbonylation compromises enzymatic activity¹⁶. OSi, which reflects the ratio of pro-oxidants to total antioxidant defenses and thereby underscores the necessity of concurrent redox balance assessment, serves as both a precise indicator of oxidative status and a valuable biomarker for OS^{17,18}. Emerging evidence highlights a significant interplay between OS and the gut microbiota, which is essential for immune response and metabolic regulation¹⁹. Individuals affected by OS-related conditions often exhibit notable alterations in the gut microbiota²⁰. For example, a study demonstrated that shifts in the gut microbiota of *Lactobacilli*, *Escherichia coli*, and *Enterococcus* in mice fed a high-fat diet are strongly correlated with OS¹⁹. Modifications in the gut microbiota may enhance the capacity of the host to produce antioxidants, providing protection against OS. Gut microbial families *Lachnospiraceae* and *Ruminococcaceae* metabolize cystine to produce reactive sulfur species, which enhance host antioxidant capacity²¹. Conversely, dysbiosis can disrupt metabolic processes, exacerbating OS and altering the composition and diversity of gut microbiota²². Integrated fecal metagenomic and blood metabolomic analysis offers a valuable approach for elucidating the mechanisms driving OS, as circulating metabolites mediate interactions between the gut microbiome and host physiology^{23–25}. However, the intricate relationships among changes in the hindgut microbiota, circulating metabolites, and OS remain poorly understood.

The potential of probiotics to enhance antioxidant defenses has garnered increasing attention. Although various probiotic strains have demonstrated significant antioxidant effects beneficial to host health, the efficacy of individual strains in augmenting antioxidant defenses is not well established, and data to support their widespread application remain limited^{26,27}. This highlights the need for further investigations relevant to the development of novel probiotics with antioxidant-enhancing properties. Advancing research in this area could lead to targeted strategies for managing OS and pave the way for new preventive and therapeutic approaches against OS-related diseases. Toward this end, we conducted a randomized study involving a cohort of postpartum dairy cows, wherein we measured blood biomarkers and calculated OSi. Based on these measurements, we categorized the cows into low (LOS) and high (HOS) OS groups. Furthermore, we performed integrated fecal metagenomic and blood metabolomic analysis to explore how the hindgut microbiota and systemic metabolites influence OS variability. We also used a murine model to

evaluate the ability of *P. succinatutens*, identified through metagenomic screening, to regulate systemic and hindgut antioxidant defenses.

Methods

Animals and sample collection

A cohort of 81 multiparous healthy Holstein cows (mean parity: 2.91 ± 1.01 , milk yield: 37.19 ± 8.93 , body condition score: 3.48 ± 0.19) was enrolled at 7 days post-calving. All cows were recruited from the Jin Yin Dao dairy farm of Beijing Sunlon Livestock Development Co., Ltd. The cows were housed under uniform conditions and fed identical diets (Supplementary Table 1). Prior to inclusion, each cow underwent a thorough veterinary examination and a review of farm health records to confirm the absence of clinical diseases, metabolic disorders, or recent antibiotic treatments. Blood samples were obtained during the morning hours, ranging from 6:00 to 8:00 a.m., via the coccygeal vein into evacuated EDTA-containing tubes. Following a 10-min centrifugation at $3000 \times g$ and 4°C , serum was isolated and preserved at -80°C pending analysis. Rectal fecal samples were collected aseptically, flash-frozen, and maintained at -80°C for later examination. The body condition score (BCS), a subjective assessment of body fat reserves typically rated on a scale of 1 (emaciated) to 5 (obese), was used to evaluate the nutritional status of the cows²⁸.

Measurement of serum biomarkers

Serum oxidative stress parameters were measured in 81 blood samples. Total oxidant status (TOS) was assessed using an assay kit (E-BC-K802-M) obtained from Elabscience Biotechnology Co., Ltd. (Wuhan, China). Briefly, the oxidative substances in the sample oxidize Fe^{2+} to Fe^{3+} in an acidic environment, forming a blue-purple complex upon strong binding with xylenol orange. The color intensity measured at 590 nm is directly proportional to the concentration of oxidative substances in the solution, enabling indirect determination of the overall oxidative status. The total antioxidant capacity (TAOC) was determined using a commercial assay kit (A015-1) from Nanjing Jiancheng Bioengineering Institute (Nanjing, China). This assay relies on the ability of different antioxidants to convert Fe^{3+} into Fe^{2+} , which then forms stable complexes with phenanthroline compounds. Colorimetry is used to assess the antioxidant capacity. Each assay kit was used according to the manufacturer's instructions. The redox balance parameters, TOS and TAOC, were evaluated together as a ratio of pro-oxidant to total antioxidant capacity (TOS/TAOC), which is known as the oxidant stress index (OSi). OSi is an accurate indication of changes in the oxidant status during the peripartum period. In our cohort of 81 dairy cows, we first examined the distribution of OSi values and calculated the 25% and 75% percentiles, which were 1.150 and 1.779, respectively. Using these percentiles as relative thresholds, we objectively defined candidate groups representing distinctly low ($\text{OSi} < 1.150$) and high ($\text{OSi} > 1.779$) OS. From these candidate groups, nine cows were randomly selected for HOS and nine for LOS to minimize selection bias (Supplementary Table 2). These 18 cows were analyzed for fecal metagenomes and serum metabolomes. A priori power analysis was performed to determine the sample size adequacy for detecting microbial differences. Based on an effect size of 0.77 from a previous study²⁹, we set $\alpha = 0.05$ and power $(1 - \beta) = 0.80$ using G*Power software (v3.1.9.7; <https://g-power.apponic.com>). The analysis indicated a minimum requirement of 16 total sample sizes, ensuring our inclusion of 18 samples was sufficient for subsequent analysis.

The serum concentrations of glutathione peroxidase (GSH-Px) (A005-1), superoxide dismutase (SOD) (A001-1), MDA (A003-1), amyloid A (H134), haptoglobin (H136), interleukin- 1β (H002-1-2), interleukin-6 (H007-1-2), tumor necrosis factor- α (H052-1-2), nonesterified fatty acids (A042-2-1), β -hydroxybutyric acid (E030-1-1), triglycerides (A110-2-1), glucose (F006-1-1), insulin (H203-1-2), insulin growth factor-1 (H041-1-2), alanine aminotransferase (C009-3-1), aspartate aminotransferase (C010-3-1), total bilirubin (C019-1-1), and alkaline phosphatase (A059-2-2) were measured using commercial diagnostic kits (Jiancheng Institute of Bioengineering, Nanjing, China) according to the manufacturer's protocols.

Measurement of short-chain fatty acid concentrations

Thawed fecal samples and colonic contents were subjected to a standardized procedure for SCFAs (acetate, propionate, and butyrate) analysis. Briefly, 1 g of solid sample was mixed with 4 mL of distilled water and subjected to centrifugation at $2500 \times g$ at ambient temperature. Following centrifugation, 1 mL of the resultant supernatant was isolated and transferred to a 1.5 mL centrifuge tube containing 0.2 mL of a deproteinizing solution composed of 25% (w/v) metaphosphoric acid (37267-86-0, Sigma) and 2 g/L 2-ethylbutyric acid (10995-9, Sigma) as the internal standard. This mixture was then incubated in an ice bath for 30 min at 4 °C, followed by a second centrifugation step at $10,000 \times g$ at 4 °C. The supernatant obtained from this step was used for the determination of SCFAs employing gas chromatography (Agilent 6890 N, Agilent Technology, Inc., USA), with detailed instrument parameters provided in Supplementary Table 3. Standard curves were established using quality control samples of acetate (A6283, Sigma), propionate (P1386, Sigma), and butyrate (B103500, Sigma).

Fecal DNA extraction, 16S rRNA gene sequencing, and data processing

Fecal genomic DNA was extracted using the Omega E.Z.N.A. Stool DNA Kit (Omega Bio-tek, Inc., USA) following the manufacturer's instructions. The concentration and quality of the extracted genomic DNA were assessed using a NanoDrop 2000 spectrophotometer (Thermo Scientific Inc., USA), and the samples were stored at -20 °C for subsequent analyses. Amplification of the V3-V4 hypervariable region of the bacterial 16S rRNA gene was conducted using universal primers 338 F (5'-ACTCCTACGGGAGG-CAGCAG-3') and 806 R (5'-GGACTACNNGGTATCTAAT-3'). The 5'-end of each primer was customized with an 8-digit barcode sequence specific to each sample (provided by Beijing Allwegene Company). Polymerase chain reaction (PCR) was performed in a 25 µL reaction volume containing 12.5 µL 2X Taq PCR MasterMix (Vazyme Biotech Co., Ltd., China), 3 µL BSA (2 ng/µL), 1 µL forward primer (5 µM), 1 µL reverse primer (5 µM), 2 µL template DNA, and 5.5 µL ddH₂O. The cycling conditions comprised an initial denaturation step at 95 °C for 5 min, followed by 28 cycles of denaturation at 95 °C for 45 s, annealing at 55 °C for 50 s, extension at 72 °C for 45 s, and a final extension at 72 °C for 10 min. The PCR products were purified using the Agencourt AMPure XP Kit (Beckman Coulter, Inc., USA). Subsequently, sequencing libraries were generated using the NEB Next Ultra II DNA Library Prep Kit (New England Biolabs, Inc., USA) following the manufacturer's recommendations. The quality of library was assessed using a Nanodrop 2000 spectrophotometer (Thermo Fisher Scientific, Inc., USA), an Agilent 2100 Bioanalyzer (Agilent Technologies, Inc., USA), and an ABI StepOnePlus Real-Time PCR System (Applied Biosystems, Inc., USA).

Deep sequencing was conducted using the Illumina MiSeq platform (Illumina, Inc., USA) at Beijing Allwegene Technology Co., Ltd. Following the sequencing run, image analysis, base calling, and error estimation were performed using the Illumina Analysis Pipeline Version 2.6 (Illumina, Inc., USA). The raw sequencing data were demultiplexed into individual samples based on barcode sequences using the QIIME software³⁰. Subsequently, raw reads were filtered and trimmed using the Pear software³¹, removing sequences with lengths less than 120 bp, quality scores below 20, or ambiguous bases. Splicing was performed with a mismatch rate of 0.1 and a minimum overlap setting of 10 base pairs. After splicing, sequences shorter than 230 bp were discarded using the Vsearch software³², and chimeric sequences were removed using the UCHIME method against the Gold Database³³. Qualified sequences were clustered into operational taxonomic units (OTUs) at a 97% similarity threshold using the Uparse algorithm in the Vsearch software³⁴. Taxonomic assignments of representative OTU sequences were performed using the BLAST tool against the Silva138 Database^{35,36}. Rarefaction curves and alpha diversity indices (Shannon and Chao1) were generated using QIIME based on the OTU data. Differences between groups were assessed using the Tukey's test. Beta-diversity distances between samples were calculated using the Bray-Curtis algorithm,

and principal coordinate analysis (PCoA) with arithmetic mean (UPGMA) clustering was conducted. Analysis of similarities (ANOSIM) with 999 permutations, implemented in the vegan package in R, was used to evaluate differences between the LOS and HOS groups. Differentially abundant taxa were identified using the Wilcoxon test, with significance set at $P < 0.05$.

Metagenomic sequencing and functional analysis

DNA was fragmented to a size of 300 bp using a Covaris ultrasonic crusher. This was followed by end repair, A-tailing, and ligation of Illumina-compatible adapters for preparing sequencing libraries. Deep sequencing of DNA libraries was conducted on an Illumina NovaSeq PE150 platform (Allwegene Company, Beijing). Post-sequencing, Illumina Analysis Pipeline Version 2.6 was utilized for image analysis, base calling, and error estimation. Fastp was used for quality control of the raw sequencing data, which involved the removal of adapter sequences and low-quality reads³⁷. Reads with more than 10% N (uncertain base) ratio, more than 50% low-quality bases ($Q \leq 10$), or exhibiting abrupt stop sequences were filtered out. The reads were then aligned to the host genome (https://www.ncbi.nlm.nih.gov/datasets/genome/GCA_021347905.1/) using the bowtie2 (v2.3) software, and those aligning to the host reference genome were excluded³⁸. Taxonomic annotation was conducted using DIAMOND (v2.0.11, <http://ab.inf.uni-tuebingen.de/software/diamond/>) to assess the microbial composition in accordance with the NCBI NR database (<https://ftp.ncbi.nlm.nih.gov/blast/db/>)³⁹. Read counts within each sample were normalized to counts per million to mitigate bias caused by variations in sequencing depth. Taxa with differential abundances were identified using linear discriminant analysis effect size (LEfSe). For functional annotation, DIAMOND was used to perform Kyoto encyclopedia of genes and genomes (KEGG) annotations against the KEGG database (<http://www.genome.jp/kegg/>), with differential KEGG pathways determined using the Wilcoxon test. Statistical significance was defined as $P < 0.05$, whereas trends were examined for values in the $0.05 < P < 0.10$ range.

Co-occurrence network construction and robustness testing

Spearman's correlation analysis (R package *psych*, v4.2.3) was performed through using the relative abundances of genera and species, retaining only correlations with $|R| > 0.5$ and $P < 0.05$ for network construction. The co-occurrence networks within LOS and HOS groups were visualized using Gephi v0.10.1 (<https://gephi.org>). Network robustness was evaluated using graph spectra. Unweighted adjacency matrices, with entries indicating binary OTU interactions, were imported into R for computational analysis. Natural connectivity was computed through eigenvalue decomposition of the adjacency matrices normalized by the total node count. In parallel, the average node degree (mean number of connections per OTU) was calculated using the *igraph* package (v2.0.3) following conversion to undirected graph objects. To systematically evaluate network robustness, iterative node removal simulations were implemented through sequential deletion of randomly selected rows and columns from adjacency matrices (1-200 iterations), followed by recalculation of natural connectivity and average degree⁴⁰. All computational outputs were compiled into a structured data-frame and visualized using *ggplot2* (v3.4.4) for comparative analysis.

Metabolomic analysis of blood samples

Serum samples (100 µL) were processed by precipitating proteins via vortexing for 30 s, followed by sonication for 10 min in an ice-water bath, and subsequent incubation for 1 h at -40 °C after adding 200 µL of extraction solution (acetonitrile:methanol = 1:1). Thereafter, the samples were centrifuged at 12,000 rpm ($RCF = 13,800 \times g$, $R = 8.6$ cm) for 15 min at 4 °C. The supernatant, thus obtained, was transferred to new glass vials for liquid chromatography-mass spectrometry (LC-MS). The blank sample was used before the first sample was injected, between every 10 samples, and after all samples were run to account for potential background interference or contamination. A quality control (QC) sample was prepared by combining equal aliquots of the supernatants from each sample to monitor the consistency of the analysis. LC-MS analysis was conducted by Beijing Allwegene

Technology Co., Ltd., using an Orbitrap Exploris 120 mass spectrometer (Orbitrap, Thermo Fisher Scientific) coupled with an ultra-high-performance liquid chromatography (UHPLC) system (Vanquish, Thermo Fisher Scientific)^{41,42}. Chromatographic separation was performed using an Acquity UHPLC system (Acquity LC, Waters) equipped with a Waters UPLC column (Acquity UPLC BEH Amide 1.8 μm , 2.1 \times 100 mm; Waters, Milford, MA). The mobile phases consisted of 25 mM ammonium hydroxide and 25 mM ammonium acetate in water (mobile phase A), and 100% ACN (mobile phase B), and the flow rate was 0.5 mL/min. The samples were maintained at 4 °C in the autosampler, and 2 μL was injected into the system. Data acquisition was controlled using Xcalibur, the acquisition software of Thermo Fisher Scientific, utilizing the capability of Orbitrap Exploris 120 mass spectrometer to acquire MS/MS spectra in information-dependent acquisition (IDA) mode. In this mode, the acquisition software continuously evaluates the full-scan MS spectrum. The ESI source parameters included collision energy settings at SNCE 20/30/40, spray voltage set at 3.8 kV (positive) or -3.4 kV (negative), sheath gas flow rate at 50 Arb, aux gas flow rate at 15 Arb, capillary temperature at 320 °C, full MS resolution at 60,000, and MS/MS resolution at 15,000.

Raw data processing, peak detection, extraction, alignment, and integration were performed using an internal program developed in R based on XCMS. ProteoWizard was used to convert the raw data to the mzXML format. Metabolite identification was performed using the R package and AllwegeneDB, resulting in the retention of X metabolites post-processing. Features corresponding to metabolites detected in less than 50% of the experimental samples were excluded from further analysis. Missing values in the raw data were imputed with half of the minimum value. Metabolite quantification was standardized using stable isotope-labeled internal standards. Raw metabolite peak areas were normalized to their corresponding internal standards peak areas to correct for variations, and features with a relative standard deviation (RSD) > 30% were excluded from subsequent analyses. The processed data, including peak number, sample name, and normalized peak area, were input into the R package MetaboAnalystR for orthogonal partial least squares discriminant analysis (OPLS-DA)⁴³. To evaluate the robustness and predictive ability of the OPLS-DA model, additional 200-times permutation testing was performed⁴⁴. The variable importance in projection (VIP) was used to identify the most influential variables contributing to the model. Compounds with VIP > 1 and $P < 0.05$ (as determined using the Student's t -test) were considered significantly altered metabolites. Furthermore, commercial databases including KEGG (<http://www.kegg.jp>) and MetaboAnalyst (<http://www.metaboanalyst.ca/>) were used for exploring the pathways of identified metabolites, which employs a hypergeometric test (over-representation analysis) to assess whether metabolites in a pathway are enriched, and pathways with $P < 0.05$ were considered significant.

Mice and experimental design

Twenty female C57BL/6 J mice, aged 8 weeks, were procured from Sibeifu Biotechnology Co., Ltd. (Beijing, China) and permitted a 7-day acclimation period before treatment. The mice were accommodated in standard specific pathogen-free animal barrier facilities under controlled conditions: room temperature (23.0 ± 2.0 °C), 50–60% relative humidity, and a 12 h light cycle daily. During this period, the animals were provided a standard diet and purified water. To deplete the gut microbiota, the mice were administered an antibiotic cocktail (1 g/L ampicillin, 1 g/L neomycin, 1 g/L metronidazole, 0.5 g/L vancomycin) dissolved in ultrapure water over 7 days^{45,46}. Mice had free access to the antibiotic-infused water and received an additional daily oral dose of 200 μL . After this treatment, a 4-day washout period was implemented to eliminate residual antibiotics. Mice were then randomly allocated into two groups ($n = 10$ per treatment, with 5 mice per cage)—the control (CON) group and the treatment (TRT) group. Mice in the CON group were administered 200 μL of phosphate-buffered saline (PBS) daily via gavage, whereas those in the TRT group were gavaged with 200 μL of *P.*

succinatutens bacterial solution (10^8 colony-forming unit (cfu)/day). Strains of *P. succinatutens* (DSM 22533) were obtained from Deutsche Sammlung von Mikroorganismen und Zellkulturen (Braunschweig, Germany) and cultivated overnight under anaerobic conditions in PYS medium. The PYS medium consists of Columbia blood agar base (KDM055) supplemented with sterile defibrinated sheep blood (KDM177) (Mingzhoubio, China). The overnight culture was diluted 100-fold with fresh PYS. Subsequently, *P. succinatutens* was anaerobically incubated for an additional 24–48 h. The CFU values were ascertained by inoculating samples onto PYS agar plates. After 14 days of treatment, mice were euthanized using carbon dioxide (CO_2) asphyxiation. CO_2 was infused into a sealed euthanasia chamber at a rate of 10–30% of the chamber's volume per min until the mice became immobile, ceased breathing, and exhibited dilated pupils. Thereafter, the CO_2 flow was stopped, and the mice were observed for an additional 2–3 min to confirm death. Colonic tissues were harvested and preserved in two forms: paraffin-embedded sections for histological analysis, and samples stored at -80°C in 5 mL cryotubes for subsequent gene and enzyme assays. Colonic contents were collected and stored at -80°C until SCFAs (acetate, propionate, and butyrate) quantification. Blood was collected from the orbital plexus of mice under light anesthesia using capillary tubes. After allowing the samples to clot at room temperature for 30 min, they were centrifuged at $3000 \times g$ for 10 min at 4 °C, and the serum was then stored at -80°C until further TAOC and TOS analysis.

Histomorphological examination of the mice colon

Colon tissue specimens were processed through a graded ethanol series for dehydration, encapsulated in paraffin, embedded in paraffin, and sectioned at 6 μm thickness. Following hematoxylin staining, the colonic morphology was inspected under an Olympus BX-51 light microscope (Olympus Corporation, Tokyo, Japan) at 10 \times magnification. An experienced pathologist performed a blinded evaluation of the tissue sections.

Assay of antioxidant enzymes in mice samples

Colon tissue samples (0.1 g) were homogenized in saline solution using an Ultra-Turrax T10 disperser (IKA Werke, Germany) and subsequently centrifuged at $3000 \times g$ for 10 min at 4 °C to isolate the supernatant for enzyme analysis ($n = 5$). The activities of glutathione peroxidase (GSH-Px; A005-1), superoxide dismutase (SOD; A001-1), MDA (A003-1), and catalase (CAT; A007-1-1) in the colon were determined using commercial diagnostic kits (Jiancheng Institute of Bioengineering) according to the manufacturer's specified protocols.

Quantitative real-time PCR (qRT-PCR) analysis of mice samples

Total RNA was isolated from colon tissue samples, and complementary DNA (cDNA) was prepared using the Taq Plus Master Mix (Vazyme, China). Primer sequences utilized in this study are listed in Supplementary Table 4. For quantitative real-time PCR, the ChamQ SYBR Color qPCR Master Mix (Vazyme, China) was employed. The PCR cycling conditions comprised an initial denaturation step at 95 °C for 5 min, followed by 35 amplification cycles consisting of 30 s at 95 °C, 30 s at 55 °C, and 1 min at 72 °C. The target genes analyzed were *Claudin-1*, *Oclcludin*, *ZO-1*, *Nrf2*, *Keap1*, and *HO-1*, with β -actin used as the housekeeping gene for normalization.

Statistical analysis

All descriptive data are presented as the mean \pm standard error of the mean (SEM). Data normality was first assessed ($\alpha = 0.05$), and all datasets followed a normal distribution ($P > 0.05$), validating the use of parametric tests. Phenotypic characteristics, concentrations of serum biomarkers, SCFAs, enzymatic activities, and gene expression in the colon were statistically analyzed using the Student's t -test in GraphPad Prism v9.4.1 (GraphPad Software, California, USA). Correlations between variables were assessed using Spearman's and random forest analyses. A significance level of $P < 0.05$ was established for statistical significance, whereas trends were examined for $0.05 < P < 0.10$.

Table. 1 | Phenotypic characteristics of dairy cows and their serum biomarker levels at 7 days postpartum (n = 9)

Items	LOS	HOS	SEM	P-value
Phenotypic characteristics				
Parity	2.67	2.78	0.43	0.80
Body condition scores	3.33	3.36	0.11	0.81
Milk yield, kg/d	38.42	39.72	2.71	0.64
Oxidative stress parameters				
Total oxidative status, μM	5.27	11.42	0.74	<0.01
Total antioxidant capacity, mM	0.73	0.47	0.05	0.01
Oxidative stress index ^a	0.72	2.52	0.11	<0.01
Superoxide dismutase, U/mL	52.48	53.14	0.98	0.76
Glutathione peroxidase, $\mu\text{mol/L}$	11.79	10.42	0.85	0.46
Malondialdehyde, nmol/mL	1.58	1.66	0.07	0.58
Inflammation parameters				
Serum amyloid A, $\mu\text{g/mL}$	23.38	24.19	0.49	0.46
Haptoglobin, ng/mL	46.38	48.65	1.05	0.32
Interleukin-1 β , ng/L	50.84	52.57	1.46	0.59
Interleukin-6, ng/L	367.73	403.18	14.70	0.26
Tumor necrosis factor- α , ng/L	217.27	229.83	7.44	0.44
Metabolic and liver function parameters				
Nonesterified fatty acids, $\mu\text{mol/L}$	39.73	41.63	1.29	0.50
β -hydroxybutyric acid, mmol/L	0.42	0.45	0.02	0.51
Triglyceride, mmol/L	0.21	0.18	0.02	0.41
Glucose, mmol/L	3.26	3.28	0.09	0.92
Insulin, mIU/L	24.59	24.59	2.60	0.67
Insulin growth factor-1, ng/mL	108.71	120.67	3.28	0.07
Alanine aminotransferase, U/L	21.91	28.18	1.92	0.11
Aspartate aminotransferase, U/L	131.33	129.64	9.19	0.93
Total bilirubin, $\mu\text{mol/L}$	2.75	2.07	0.35	0.36
Alkaline phosphatase, g/L	38.81	39.61	2.45	0.88

^aThe oxidative stress index is calculated as the ratio of total oxidative status to total antioxidant capacity.

Results

Basic characteristics of the dairy cows used in this study

Table 1 summarizes the key phenotypic characteristics and levels of serum biomarkers in the HOS and LOS groups. No statistically significant discrepancies were detected among the groups with respect to milk yield, parity, BCS, inflammation parameters, or metabolic and liver function parameters. However, distinct variations were evident in the serum OS markers. Specifically, the LOS group exhibited higher serum TAOC levels compared to those in the HOS group ($P = 0.05$). Conversely, the serum TOS and OSI levels exhibited a significant reduction in the LOS group relative to the HOS group ($P < 0.01$). These findings underscore the potential role of serum OS parameters in distinguishing between the HOS and LOS groups and highlight the relevance of these markers in assessment of OS.

Altered fecal bacterial community in postpartum cows during OS

A total of 2195 OTUs were identified at a nucleotide sequence identity threshold of 97% among the sequencing reads (Supplementary Data 1). Beta diversity analysis revealed distinct clustering of the LOS and HOS cow samples into separate groups [$P = 0.001$, analysis of similarity (ANOSIM) $R = 0.806$] (Fig. 1a). Alpha diversity analysis indicated significantly higher Chao1 and Shannon indices in the LOS group than in the HOS group (Fig. 1b). The most abundant bacterial phyla across all samples were Firmicutes and Bacteroidetes (Fig. 1c). The relative abundance of Spirochaetota, Fibrobacterota, and Cyanobacteria was significantly higher ($P < 0.01$) in the LOS group, whereas that of Bacteroidetes was not significantly different (Fig. 1c). At the genus level, the 20 most abundant genera represented 82.4% of

the overall abundance, with *Oscillospiraceae* UCG 005 being the most prevalent across samples (Fig. 1d). Notably, the relative abundance of *Oscillospiraceae* UCG 005 was significantly lower ($P < 0.001$), whereas that of *Lachnospiraceae* UCG 008, *Treponema*, *Ruminiclostridium*, and *Deffluviitaleaceae* UCG 011 was significantly higher ($P < 0.001$) in the LOS group (Fig. 1d, Supplementary Data 2).

Co-occurrence network of genera was constructed to assess the microbial interactions between the two groups. The results indicated that the LOS microbial network exhibited more intricate interactions, characterized by a greater number of nodes (325 vs. 306, Fig. 2a) and edges (277 vs. 266, Fig. 2b). Robustness testing further revealed that the LOS network maintained greater stability upon random node removal, as evidenced by higher average degree (Fig. 2c) and natural connectivity (Fig. 2d) compared to the HOS network.

Metagenomic analysis reveals key species associated with OS

Metagenomic sequencing yielded a total of 2,708,436,322 reads from 18 fecal samples of cows, with an average of $23,153,246 \pm 9,427,001$ reads per sample. The fecal microbiome of cows predominantly comprised bacteria ($97.90 \pm 0.06\%$), with minor proportions of eukaryotes ($0.04 \pm 0.01\%$), archaea ($1.00 \pm 0.08\%$), and viruses ($1.10 \pm 0.03\%$). At the species level, the predominant bacteria observed in all samples were *Firmicutes bacterium* CAG110, *Clostridiales bacterium*, *Oscillospiraceae bacterium*, and *Bacteroides* sp. CAG709 (Fig. 3a), with *Firmicutes bacterium* CAG110 being the most prevalent across samples (Fig. 3a). The signature fecal microbiota at the species level in the LOS and HOS groups was identified using LEfSe

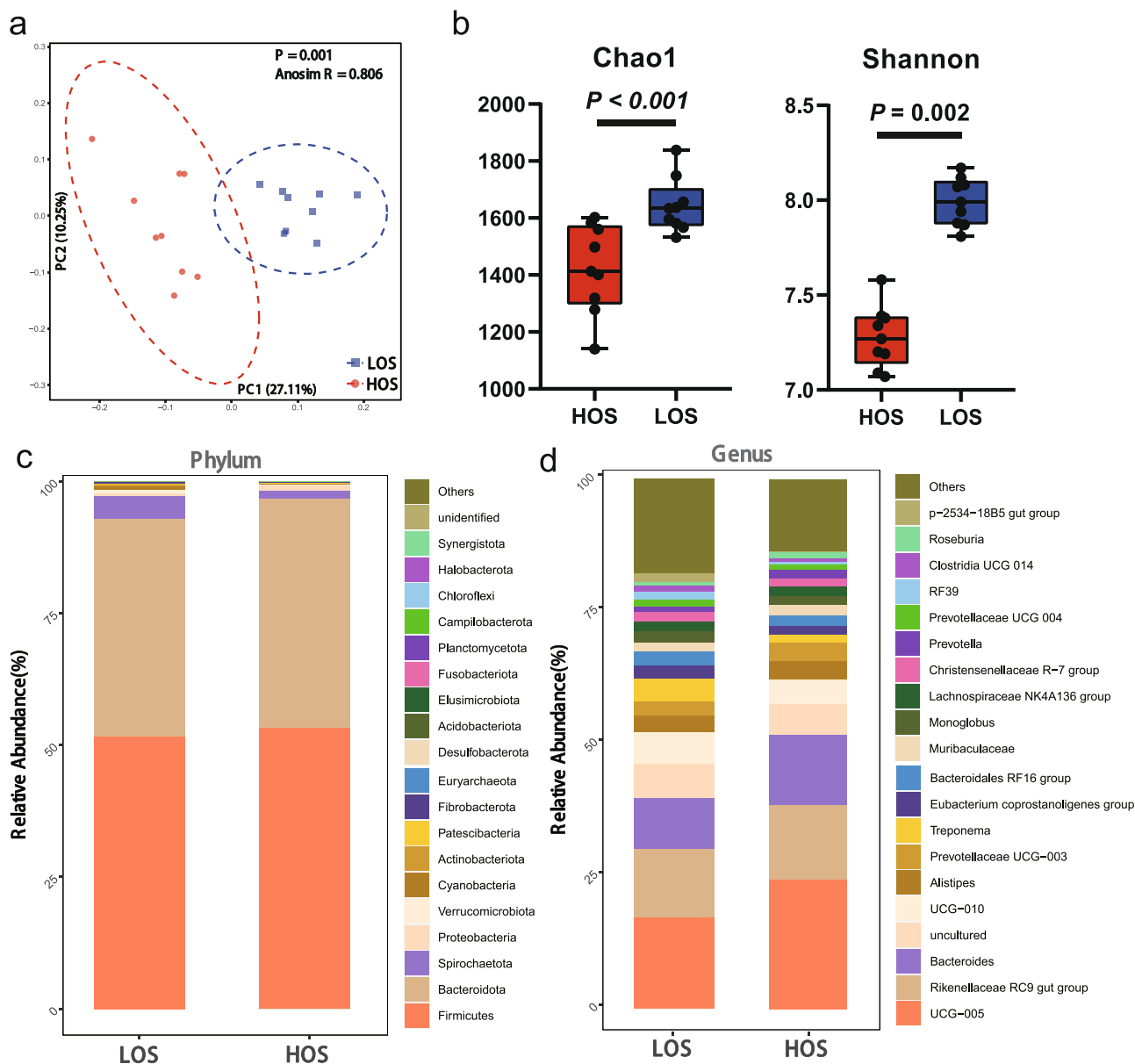


Fig. 1 | Hindgut microbial diversity in cows based on the 16S rRNA gene sequencing data (n = 9). **a** The PCoA of the Bray-Curtis distances of the fecal microbiome between the LOS and HOS groups. **b** The Shannon and Chao1 indices of the fecal microbiome between the LOS and HOS groups. **c** Relative abundance of phyla between the LOS and HOS groups. **d** Relative abundance of genera between

the LOS and HOS groups. Differences in alpha diversity between groups were assessed using Tukey's test. Beta-diversity distances were calculated using the Bray-Curtis algorithm. PCoA with UPGMA clustering was performed. ANOSIM with 999 permutations was used to evaluate differences between the LOS and HOS groups. The significance threshold was set at $P < 0.05$.

($P < 0.05$, LDA > 2.5) (Fig. 3b and c, Supplementary Table 5). The predominant signature species of the HOS group belonged to the genus *Firmicutes*, and included *Firmicutes bacterium* CAG110 56 8, *Firmicutes bacterium* CAG110, and *Firmicutes bacterium* CAG137. Additionally, *unclassified Faecalibacterium* was a signature of the HOS group, whereas *Bacteroidetes bacterium*, *Treponema bryantii*, *P. succinatutens*, *Paludibacter propionigenes*, and *Clostridium* sp. CAG413 were signatures of the LOS group. Spearman's correlation analysis was conducted for the OS parameters (T-AOC, TOS, and OSI) and signature microbial species that met the screening conditions. Most of these species exhibited significant negative correlations with OSI (Fig. 3d). Notably, species such as *Clostridium* sp. CAG413 ($R = -0.83$, $P < 0.01$), *Bacteroidetes bacterium* ($R = -0.80$, $P < 0.01$), *P. succinatutens* ($R = -0.53$, $P = 0.02$), and *Paludibacter propionigenes* ($R = -0.51$, $P = 0.03$) displayed negative correlations with OSI of cows. In contrast, *Firmicutes bacterium* CAG110 56 8 ($R = 0.82$, $P < 0.01$), *Firmicutes bacterium* CAG110 ($R = 0.81$, $P < 0.01$), and *Firmicutes*

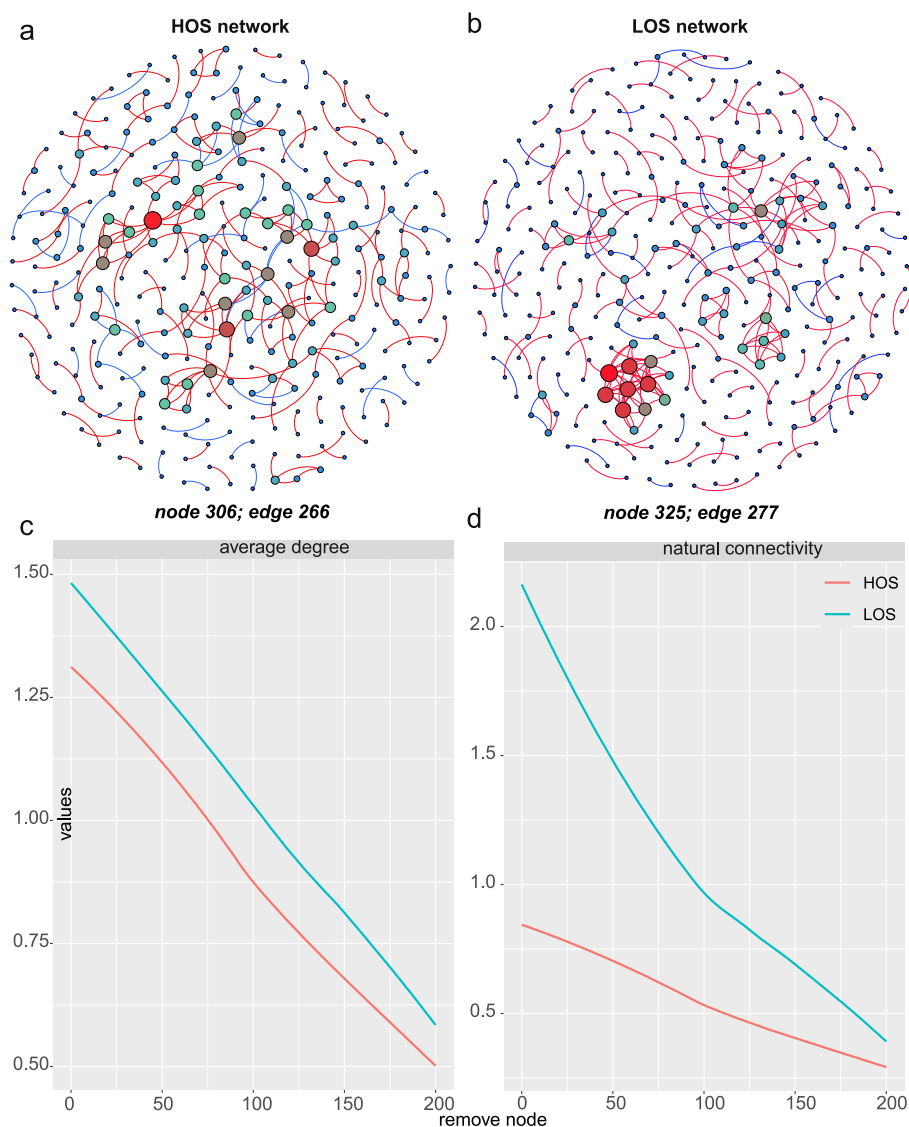
bacterium CAG137 ($R = 0.75$, $P < 0.01$) were positively correlated with OSI (Supplementary Table 6).

Moreover, we constructed a bacterial interaction network for the top 50 most abundant bacteria at the species level in both groups to elucidate the associations among these dominant bacteria. Consistent with the genus-level network, the species in the LOS group displayed more frequent interactions (Fig. 4a and b). Additionally, by analyzing the degree and closeness of each species within the LOS network, we identified key hub nodes, including *Fibrobacteres bacterium* CG2 30 45 31, *Treponema* sp. JC4 and *Treponema bryantii*, which exhibited direct and universal correlations with other nodes (Fig. 4c).

Linking key species function to OS and SCFAs dynamics

A KEGG-based functional analysis of the fecal metagenome identified 422 pathways (Supplementary Data 3). Among these, 54 KEGG pathways for metabolism were mainly perturbed between the LOS and HOS groups

Fig. 2 | The interaction network of microbial genera in the HOS and LOS groups. **a** The co-occurrence network of microbial genera in the HOS group. **b** The co-occurrence network of microbial genera in the LOS group. Nodes are sized and colored by their degree, while edges are thickened based on R value magnitude and colored red for positive or green for negative correlation. **c** The average degree of networks in the two groups. **d** The natural connectivity of networks in the two groups.



($P < 0.10$) (Fig. 5a). The most statistically significant pathways were associated with lipid metabolism, amino acid metabolism, and SCFAs metabolism. Specifically, glycerophospholipid metabolism ($P < 0.01$), D-alanine metabolism ($P < 0.01$), and secondary bile acid biosynthesis ($P < 0.01$) were significantly increased in the HOS group, while lysine degradation ($P < 0.01$), butanoate metabolism ($P < 0.01$), and propanoate metabolism ($P < 0.01$) were significantly increased in the LOS group. Building upon these findings, pathways linked to lipid metabolism (glycerophospholipid metabolism, $P < 0.01$), SCFAs metabolism (butanoate metabolism, $P < 0.01$), bile acid metabolism (secondary bile acid biosynthesis, $P = 0.01$), methionine synthesis (cysteine and methionine metabolism, $P = 0.01$), and glutathione synthesis (glutathione metabolism, $P = 0.02$) were selected for further analysis due to their functional importance in OS^{47–51}. Notably, four pathways related to SCFAs production were substantially influenced by the signature microbial species. Specifically, these species accounted for 65.34%, 60.5%, 38.0%, and 34.39% of the variation in butanoate metabolism ($P < 0.01$), beta-alanine metabolism ($P < 0.05$), propanoate metabolism ($P < 0.01$), and pyruvate metabolism ($P = 0.05$), respectively (Fig. 5b). Five microbial species, including *P. succinatutens*, *Paludibacter propionigenes*, *Bacteroides bacterium*, *unclassified Bacteroidetes*, and *Clostridium* sp. CAG413 acted as generalists in predicting these pathways ($P < 0.05$) (Fig. 5b, Supplementary Table 7).

Metabolic pathway analysis revealed that enzymes involved in SCFAs metabolism were altered in response to OS. Six enzymes (3-hydroxybutyryl-

CoA dehydrogenase, 3-hydroxyacyl-CoA dehydrogenase, butyryl-CoA dehydrogenase, phosphate butyryltransferase, butyrate kinase, and enoyl-CoA hydratase) were upregulated in butanoate metabolism. Similarly, in propanoate metabolism, enzymes such as butyryl-CoA dehydrogenase, succinyl-CoA:acetate CoA-transferase, acetate-CoA ligase alpha subunit, propionyl-CoA synthetase, succinyl-CoA synthetase alpha subunit, methylmalonyl-CoA epimerase, methylmalonyl-CoA mutase, and propionyl-CoA carboxylase alpha subunit, were more abundant in the LOS group. In pyruvate metabolism, enzymes such as pyruvate dehydrogenase E1 component, pyruvate dehydrogenase E2 component, propionyl-CoA carboxylase alpha subunit, formate C-acetyltransferase, acetyl-CoA C-acetyltransferase, acetate kinase, propionate CoA-transferase, succinyl-CoA:acetate CoA-transferase, acetyl-CoA hydrolase, acetyl-CoA synthetase, and acetate-CoA ligase subunit alpha, were more abundant in the LOS group. Furthermore, the levels of enzymes involved in beta-alanine metabolism, such as 4-aminobutyrate aminotransferase and enoyl-CoA hydratase, were also increased in the LOS group. In addition, our analysis demonstrated that the concentrations of acetate (25.50 ± 3.72 vs. 12.90 ± 2.24), propionate (9.92 ± 1.01 vs. 6.73 ± 0.65), and butyrate (4.41 ± 0.66 vs. 2.35 ± 0.48) were significantly higher in the LOS group compared to those in the HOS group ($P < 0.05$). These findings strongly support that the upregulation of enzymes in the LOS group is associated with increased production of SCFAs, underscoring the functional relevance of the observed metabolic pathway alterations (Fig. 6, Supplementary Table 8).

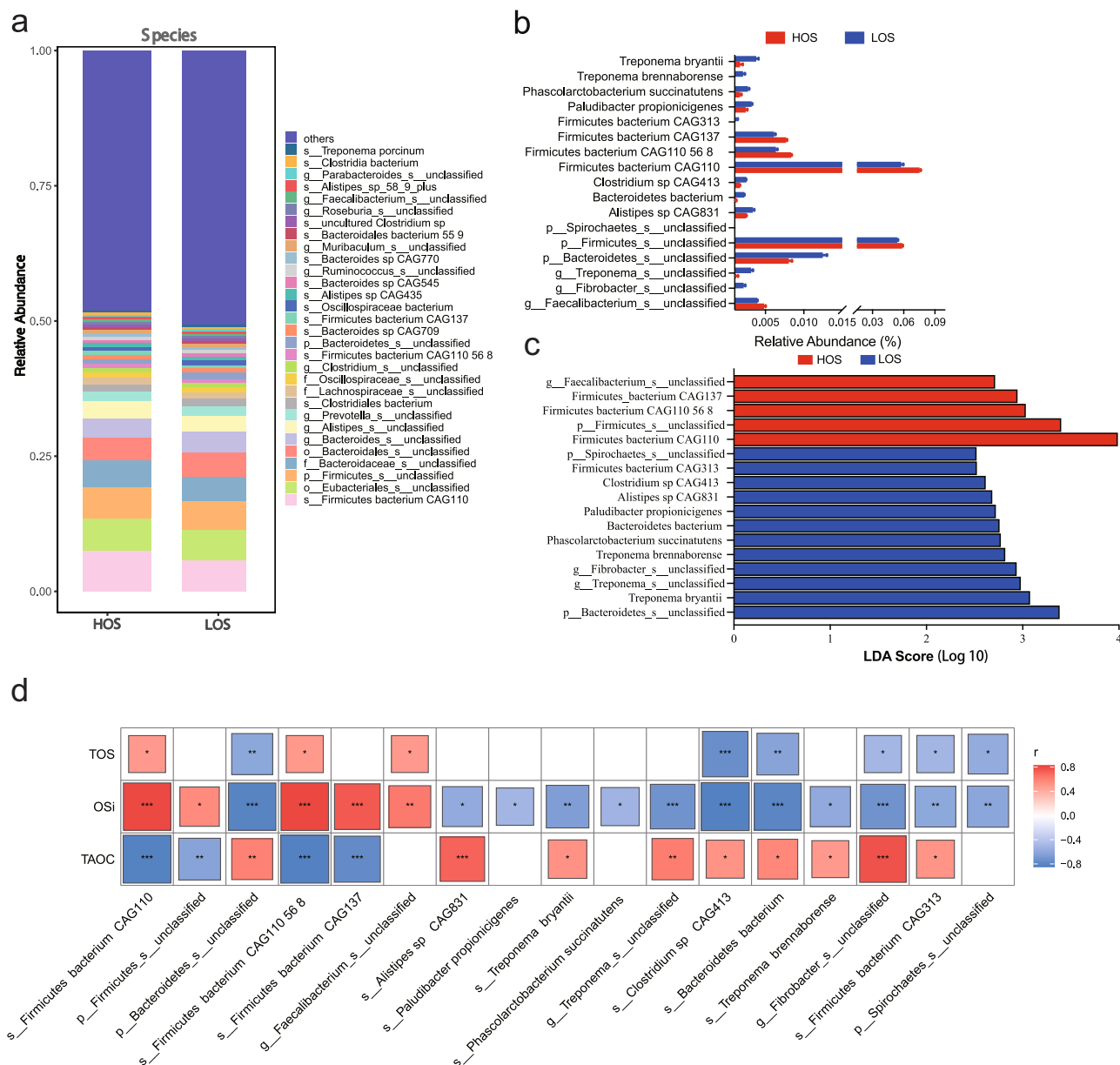


Fig. 3 | Association of altered hindgut microbial species and oxidative stress parameters according to metagenomic sequencing data (n = 9). **a** Relative abundance of the fecal microbiome at the species level in the LOS and HOS groups. **b** Identification of the signature species in the LOS and HOS groups using linear

discriminant analysis (LDA) effect size ($P < 0.05$, $LDA > 2.5$). **c** Relative abundance of the signature species in the LOS and HOS groups. **d** Signature microbial species linked to oxidative stress parameters. Correlations between variables were tested by Spearman's analysis. * $P < 0.05$, ** $P < 0.01$, *** $P < 0.001$.

Alterations in serum metabolite levels in cows with different degrees of OS

Previous studies have established a close relationship between blood metabolites and gut microbiota^{52–54}. A nontargeted LC-MS-based metabolomics approach was employed to elucidate the serum metabolites and explore their connections with the hindgut microbiome. OPLS-DA revealed a distinct clustering of LOS and HOS cows, indicating clear metabolic differences between the two groups (Fig. 7a). In a pool of 1,595 measured metabolites, 113 were significantly different ($P < 0.05$) (Fig. 7b, Supplementary Data 4). LOS cows exhibited notable increases in 1-phenyl-1H-pyrazole-5-carboxylic acid, kynurenine, 5-hydroxyindole-3-acetic acid, 2-oxindole-3-acetate, isovaleric acid, valeric acid, and formyl-5-hydroxykynurenine but significantly decreased ciprostone, 1,2-diacytylhydrazine, and mantabegron levels ($P < 0.01$) (Fig. 7c). KEGG pathway analysis revealed significant alterations ($P < 0.01$) in multiple metabolites involved in tryptophan metabolism, specifically kynurenine ($P = 0.004$,

$FC = 1.58$), 5-hydroxyindole-3-acetic acid ($P = 0.006$, $FC = 1.51$), and formyl-5-hydroxykynurenine ($P = 0.008$, $FC = 1.48$) (Fig. 7d, Supplementary Table 9). Spearman's correlation analysis revealed correlations between specific bacterial species and circulating metabolites involved in tryptophan metabolism ($P < 0.05$) (Fig. 7e, Supplementary Table 10). *Akkermansia glycaniphila*, *Azospirillum* sp. 51 20, *unclassified Acetobacter*, and *Treponema socranskii* were positively correlated, whereas *Faecalibacterium prausnitzii*, *Firmicutes bacterium CAG137*, *Firmicutes bacterium CAG110 56 8*, *Streptomyces* sp. Tu6071, and *Firmicutes bacterium CAG110* were negatively correlated ($P < 0.05$) (Fig. 7e, Supplementary Table 11). These findings underscore the strong association between altered tryptophan metabolism and OS.

For more in-depth understanding of the intricate interplay between hindgut microbial dysbiosis linked to OS and perturbations in tryptophan metabolism, we employed random forest analysis to elucidate the variance explained by microbial species. We found that the signature microbial

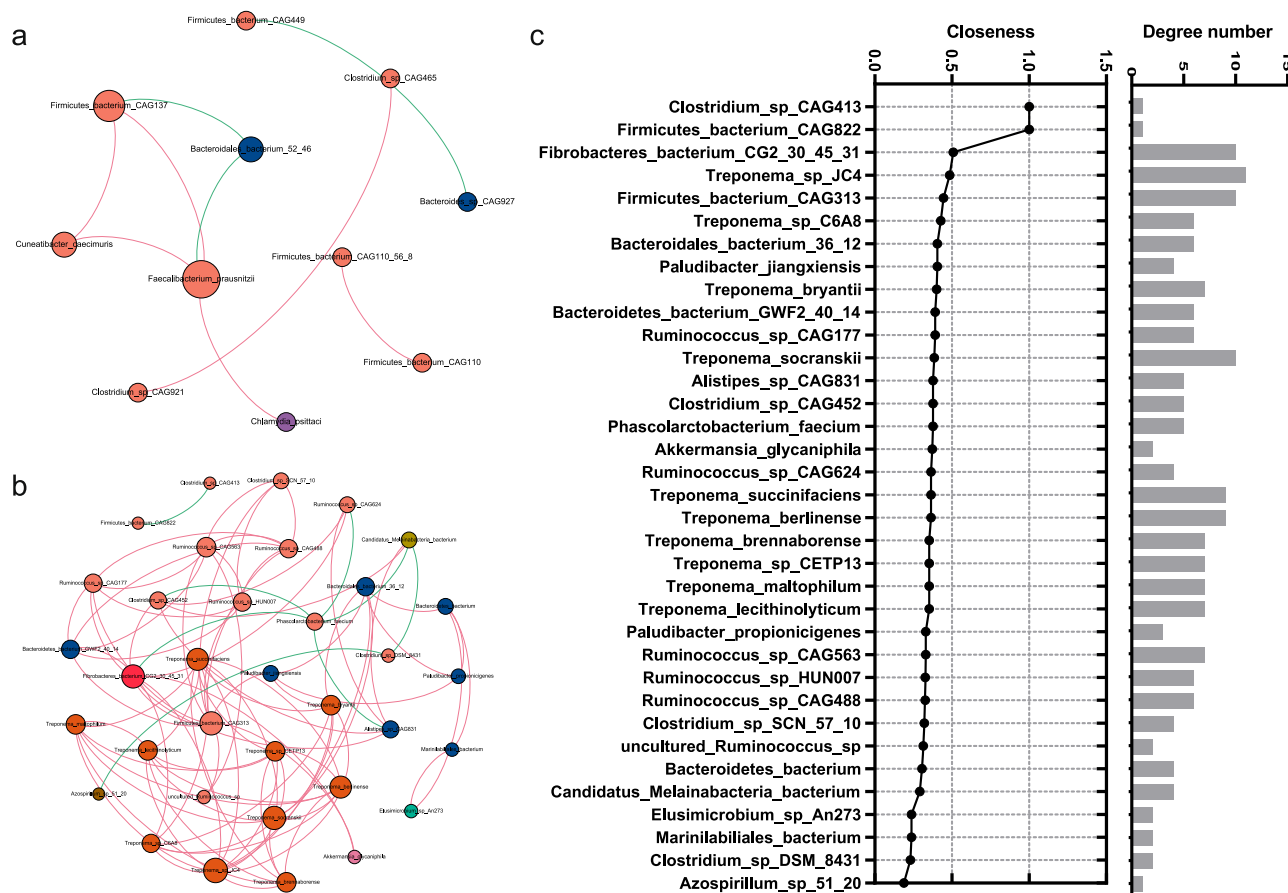


Fig. 4 | Interaction network based on the top 50 bacterial species. a The interaction network of HOS species. **b** The interaction network of LOS species. Nodes are sized by their degree and colored by node grouping, while edges are thickened based on R

value magnitude and colored red for positive or green for negative correlation. Only $P < 0.05$ and the correlation coefficient $> |0.5|$ for the top 50 most abundant species are retained. **c** The closeness and degree of species in the LOS network.

species contributed substantially to the variability observed in the key tryptophan metabolites. Specifically, these species accounted for 44.50%, 14.40%, and 7.08% of the variation in kynurenine, 5-hydroxyindole-3-acetic acid, and formyl-5-hydroxykynurenamine (Fig. 7e). Notably, certain microbial species emerged as pivotal generalists in predicting these metabolites (Fig. 7e, Supplementary Table 12), including *Azospirillum* sp. 51_20, *Ruminococcus* sp. CAG624, *Faecalibacterium prausnitzii*, *Firmicutes bacterium* CAG110_56_8, *Firmicutes bacterium* CAG110, *Streptomyces* sp. Tu6071, *Firmicutes bacterium* CAG449, unclassified *Alphaproteobacteria*, and unclassified *Bacteroidetes* (Fig. 7e, Supplementary Table 12). These results underscore the intricate relationship between substantial shifts in the hindgut microbial composition and critical metabolites in tryptophan metabolism. They provide compelling evidence supporting the notion that alterations in tryptophan metabolism induced by hindgut microbiota play a pivotal role in the onset of OS.

***P. succinatutens* administration increased host antioxidant capacity and colon integrity in mice**

To assess the potential antioxidant effects of *P. succinatutens*, female C57BL/6 J mice were administered *P. succinatutens* (10^8 cfu/day) for two weeks (Fig. 8a). The selection of *P. succinatutens* was based on its status as a signature species within the LOS group and its substantial contribution to SCFAs metabolism in this study. Additionally, drawing from a previous study indicating low levels of *P. succinatutens* in the gut of swine under OS^{55,56}, we also took into account its role in mitigating microbial dysbiosis, restoring microbial equilibrium, and its prospective therapeutic applications⁵⁷. Our findings indicated that oral administration of *P. succinatutens* significantly

increased serum TAOC levels in the TRT group compared to the CON group ($P < 0.05$, Fig. 8b). Concurrently, serum TOS levels ($P = 0.05$) and OSI ($P = 0.01$) were markedly lower in the TRT group (Fig. 8b). Histological analysis of the colon (Fig. 8f) showed that the TRT group exhibited substantial improvements in the colonic architecture with well-preserved, neatly organized crypt structures, which were further assessed via the expression of *Claudin-1* and *Occludin* genes. As indicated in Fig. 8d, both genes were significantly upregulated in the colon of TRT mice compared to CON mice ($P < 0.05$).

***P. succinatutens* upregulated the expression of antioxidant genes, enzyme activities, and SCFA concentrations in the colon of mice**

To further elucidate the antioxidant mechanisms, we examined the nuclear factor (erythroid-derived)-like 2 (Nrf2) signaling pathway in the colon tissue. As expected, the expression of Kelch-like ECH-associated protein 1 (*Keap1*) (0.94 ± 0.22 vs. 1.83 ± 0.23), which negatively regulates *Nrf2*, was significantly downregulated in the TRT group ($P < 0.05$, Fig. 8d), whereas *Nrf2* (1.99 ± 0.38 vs. 1.03 ± 0.15) and its downstream target, heme oxygenase 1 (*HO-1*) (1.50 ± 0.29 vs. 0.82 ± 0.07), were notably upregulated upon *P. succinatutens* administration ($P < 0.05$, Fig. 8d). Enzymatic assays corroborated these molecular findings, revealing significantly increased activities of GSH-Px (337.0 ± 106.0 vs. 88.30 ± 11.80) and SOD (75.20 ± 4.02 vs. 201.0 ± 45.60) in the colon tissue in the TRT group ($P < 0.05$, Fig. 8e). Besides, acetate (48.38 ± 4.62 vs. 33.12 ± 2.76) and propionate (4.75 ± 0.15 vs. 3.52 ± 0.41) concentrations in the TRT group were significantly higher than in the CON group ($P < 0.05$, Fig. 8c).

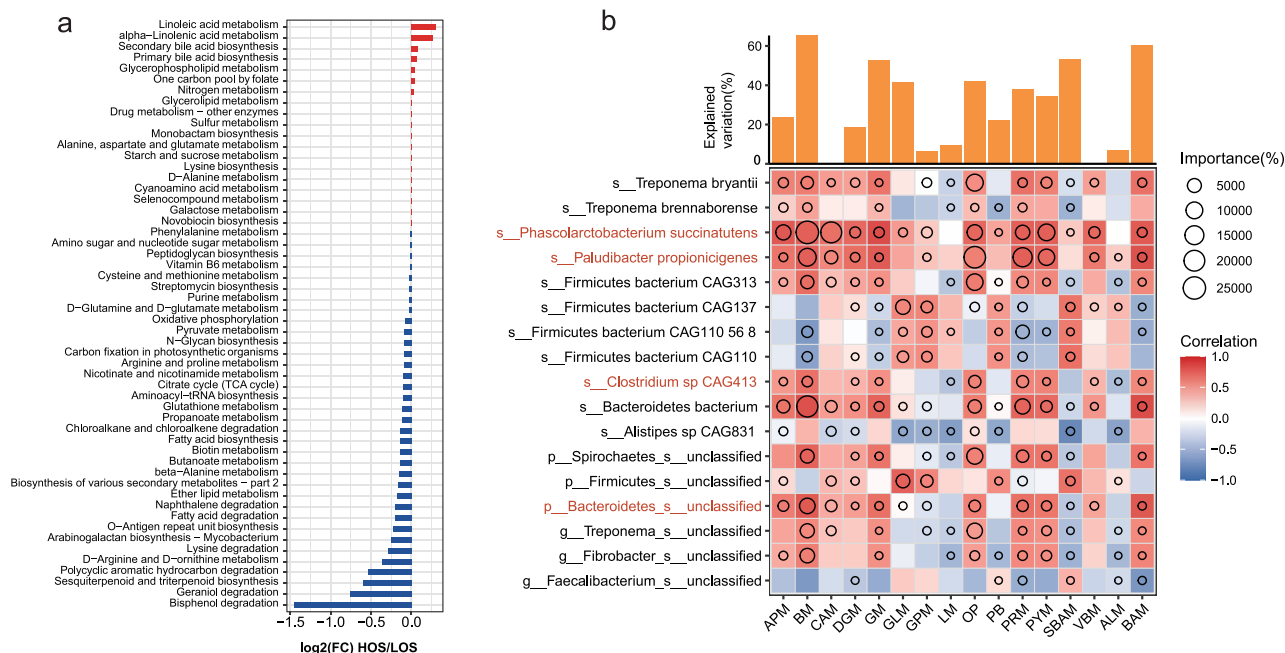
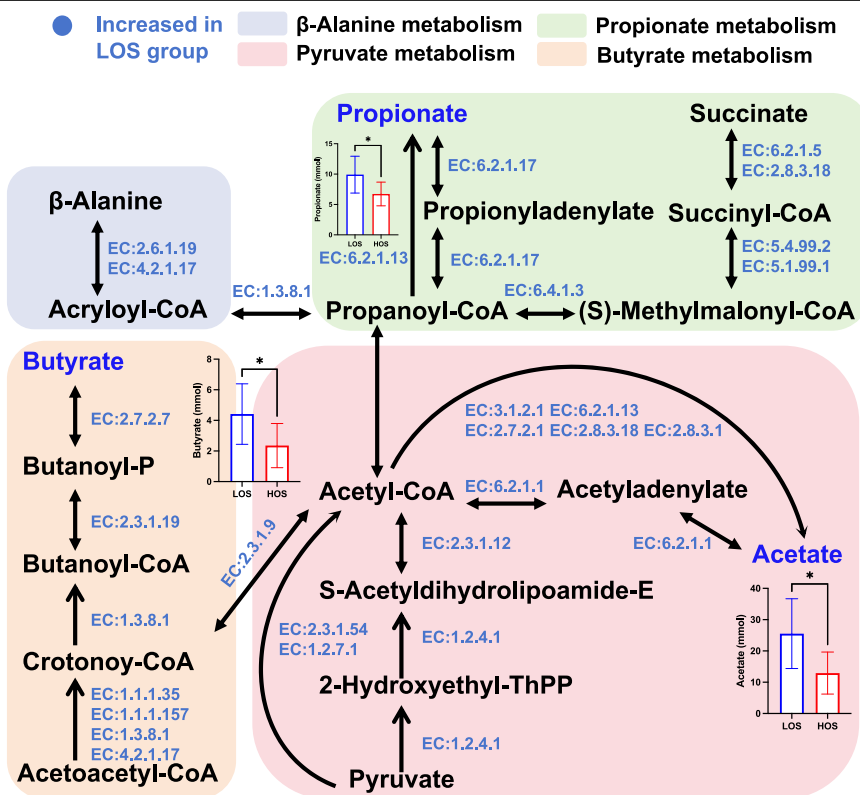


Fig. 5 | Significance of key microbial species involved in functional KEGG pathways (n = 9). **a** Hindgut microbiota KEGG pathways for metabolism that were perturbed between the HOS and LOS groups ($P < 0.10$), along with the average transcripts per million for each pathway in each group. P values calculated using the Wilcoxon test. **b** Spearman's correlations between altered fecal microbial species and their impact on functional KEGG pathways (level C). The circles overlaid on diamonds represent the significance of individual microbial species. The bar chart summarizes the total explained variations in microbial species, integrating this information with the heatmap. APM, BM, CAM, DGM, GM, GLM, GPM, LM, OP,

PB, PRM, PYM, SBAM, VBM, ALM, and BAM denote arginine and proline metabolism, butanoate metabolism, cysteine and methionine metabolism, D-glutamine and D-glutamate metabolism, glutathione metabolism, glycerolipid metabolism, glycerophospholipid metabolism, linoleic acid metabolism, one carbon pool by folate, oxidative phosphorylation, primary bile acid biosynthesis, propanoate metabolism, pyruvate metabolism, secondary bile acid biosynthesis, vitamin B6 metabolism, alpha-linolenic acid metabolism, and beta-alanine metabolism, respectively. Signature bacteria names are labeled red.

Fig. 6 | Metabolic networks of the hindgut microbiome based on metagenomic data (n = 9).

The metabolic pathways are presented based on information from the KEGG database. The SCFAs (acetate, propionate, and butyrate) measured in this study are represented in dark blue font, and the EC numbers indicate the enzyme whose genes were enriched in the hindgut in the LOS group. EC numbers and corresponding enzyme names: EC:1.1.1.157: 3-hydroxybutyryl-CoA dehydrogenase; EC:1.1.1.35: 3-hydroxyacyl-CoA dehydrogenase; EC:1.2.4.1: pyruvate dehydrogenase E1 component; EC:1.2.7.1: pyruvate ferredoxin oxidoreductase alpha subunit; EC:1.3.8.1: butyryl-CoA dehydrogenase; EC:2.3.1.12: pyruvate dehydrogenase E2 component; EC:2.3.1.19: phosphate butyryltransferase; EC:2.3.1.54: formate C-acetyltransferase; EC:2.3.1.9: acetyl-CoA C-acetyltransferase; EC:2.6.1.19: 4-aminobutyrate aminotransferase; EC:2.7.2.1: acetate kinase; EC:2.7.2.7: butyrate kinase; EC:2.8.3.1: propionate CoA-transferase; EC:2.8.3.18: succinyl-CoA:acetate CoA-transferase; EC:3.1.2.1: acetyl-CoA hydrolase; EC:4.2.1.17: enoyl-CoA hydratase; EC:5.1.99.1: methylmalonyl-CoA epimerase; EC:5.4.99.2: methylmalonyl-CoA mutase; EC:6.2.1.1: acetyl-CoA synthetase; EC:6.2.1.13: acetate-CoA ligase subunit alpha; EC:6.2.1.17: propionyl-CoA synthetase; EC:6.2.1.5: succinyl-CoA synthetase alpha subunit; EC:6.4.1.3: propionyl-CoA carboxylase alpha subunit.



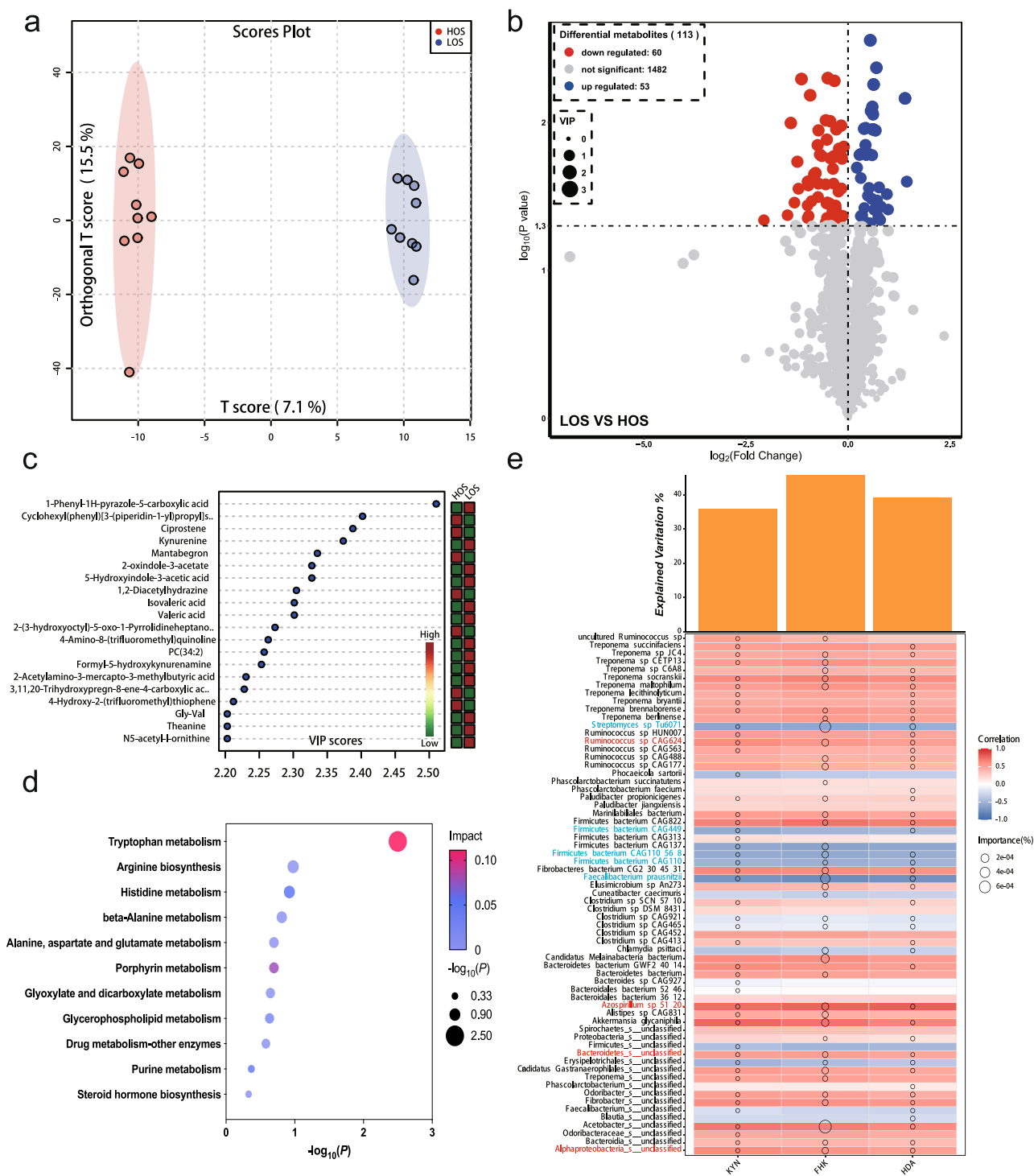


Fig. 7 | Serum metabolomic profiles in LOS and HOS cows (n = 9). **a** OPLS-DA scores plot of the serum metabolome. **b** Volcanic plot of differential serum metabolites in the LOS and HOS (control) groups. Metabolites in the LOS group compared with those in the HOS group showed varying degrees of up- or down-regulation (red and blue, respectively) ($P < 0.05$). **c** VIP score scatter plot of the top 20 differential metabolites between LOS and HOS groups ($P < 0.05$). Colors denote up-regulation (red) or down-regulation (green) in corresponding group. **d** The KEGG enrichment analysis bubble chart. Each bubble represents a metabolic pathway. The bubble size indicates pathway significance, and its color reflects the pathway impact

value from topology analysis. Lighter colors denote lower impact, and darker colors denote higher impact. **e** Spearman's correlations between altered signature microbial species and their impact on differential serum metabolites. The circles superimposed on diamonds represent the significance of individual microbial species. The bar chart summarizes the total explained variations of microbial species, integrating this information with the heatmap. KYN, FHK, and HDA denote the kynurenine, formyl-5-hydroxykynurenine, and 5-hydroxyindole-3-acetic acid, respectively. Signature bacteria names are labeled red.

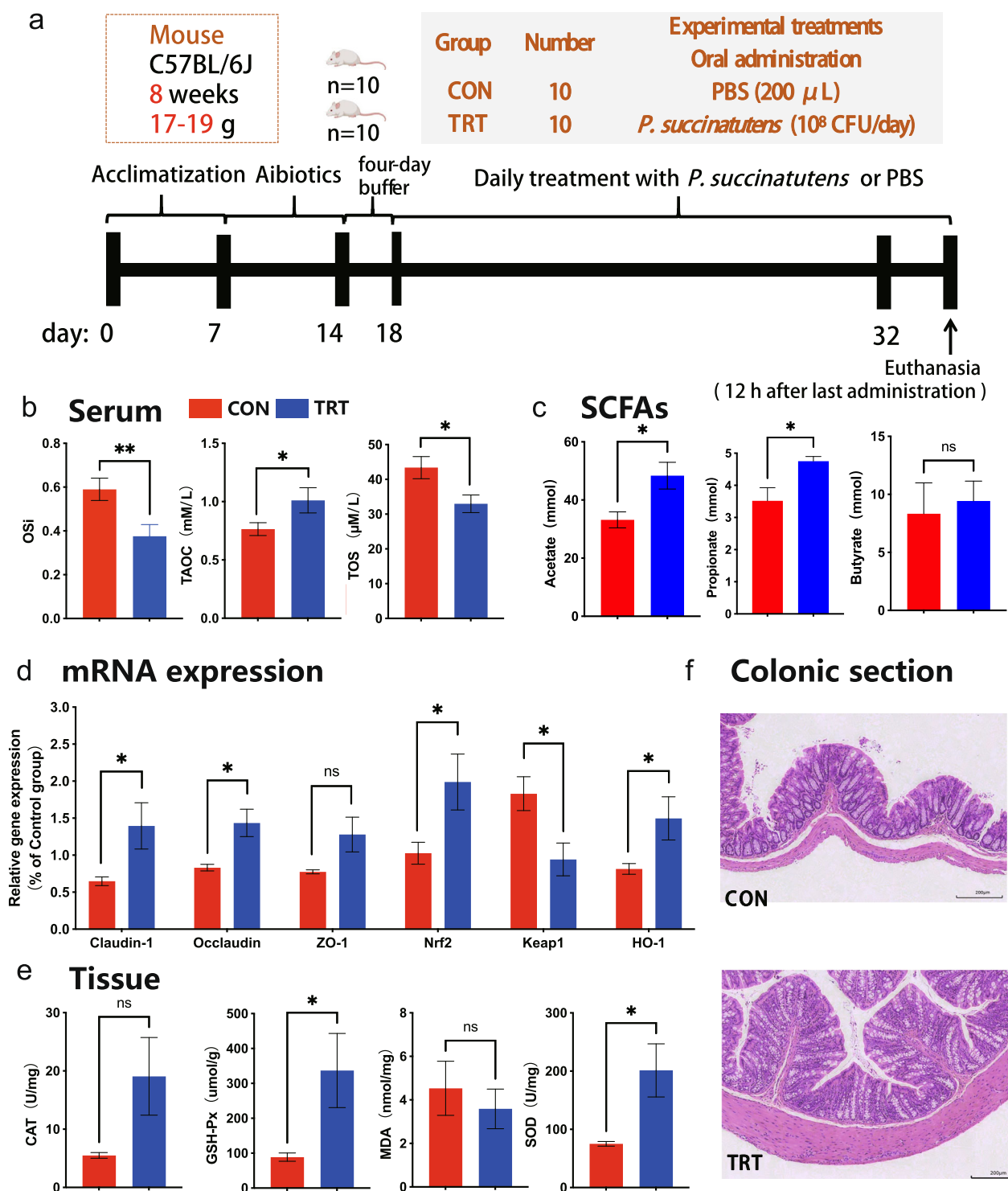


Fig. 8 | Effects of *P. succinatutens* administration on host antioxidant capacity, colonic gene expression, and enzyme activity in mice (n = 5). a Experimental design. **b** Serum oxidative stress parameters. **c** Short-chain fatty acid concentrations in colonic contents. **d** Relative expression of genes related to colon integrity and the

Nrf2 pathway. **e** Activities of superoxide dismutase (SOD), glutathione peroxidase (GSH-Px), catalase (CAT), and malondialdehyde (MDA) in the colon tissue.

f Representative H&E staining of colon sections from each group, observed at 100 \times magnification. Scale bar, 200 μ m. * P < 0.05, ** P < 0.01.

Discussion

The precise mechanisms through which the gut microbiota and metabolites contribute to the development of OS remain unclear. Given that the gut microbiota exerts multifaceted effects on host physiology, primarily through microbial metabolites, we investigated the functional profiles of complex bacterial communities in postpartum cows experiencing OS. This analysis involved integrating fecal

metagenomic sequencing data with blood metabolite analysis⁵⁸. Our dual-omics approach revealed alterations in immunometabolism, characterized by modifications in tryptophan metabolism and the disruption of SCFAs production, orchestrated by the hindgut microbiota. These findings indicated that tryptophan metabolism and SCFAs synthesis are influenced by the hindgut microbiome associated with OS, which potentially contributes to OS onset.

An essential function of tryptophan metabolism is regulation of redox homeostasis⁵⁹. A previous study demonstrated that tryptophan intervention effectively mitigates D-galactose-induced OS in mice, concurrently elevating serum SOD levels, indicating the crucial involvement of tryptophan-mediated antioxidant mechanisms in regulating systemic OS⁶⁰. Among these metabolites, kynurenine has emerged as a central player that exerts pleiotropic effects by modulating redox homeostasis. Its diverse functions include induction of antioxidant enzymes, regulation of reactive oxygen species (ROS) levels, activation of AhR and Nrf2 signaling pathways, and prevention of cellular apoptosis. Interestingly, systemic OS varied between LOS and HOS cows, yet no significant differences were detected in antioxidant enzymes (SOD, GSH-Px). This temporal uncoupling between OS and enzymatic compensation is consistent with observations in periparturient cows, where lipid peroxidation peaks precede the subsequent rise in SOD and GSH-Px activities⁶¹. Similarly, studies reported declining TAOC alongside increased SOD and GSH-Px activities in cows during metabolic transitions^{62,63}, suggesting that enzymatic systems are selectively preserved or upregulated to counteract persistent OS. However, the absence of significant enzymatic antioxidant variations may reflect compensatory activation of non-enzymatic antioxidant mechanisms and signaling pathways, as exemplified by kynurenine's capacity to scavenge free radicals and amplify cellular antioxidant defenses via glutathione and AhR-Nrf2 signaling. For example, previous studies demonstrated that kynurenine-induced glutathione upregulation serves as a critical nonenzymatic defense mechanism against ROS accumulation⁶⁴. This metabolite exhibits direct free radical-scavenging capacity, effectively neutralizing both superoxide anions ($O_2^{\cdot-}$) and H_2O_2 ⁶⁵, and further counteracts counteracting peroxynitrite ($ONOO^{\cdot-}$)-mediated oxidative damage in neural tissues⁶⁶. Recent research elucidated the pivotal function of the tryptophan-AhR signaling axis in maintaining host homeostasis. As an endogenous AhR ligand, kynurenine not only modulates ROS levels through receptor activation⁶⁷, but also engages in crosstalk with the Nrf2 pathway. This interaction promotes the transcriptional upregulation of antioxidant enzymes like heme oxygenase-1 (HO-1), thereby amplifying cellular defense systems. Consequently, the delicate balance between the kynurenine-mediated pro-oxidant and antioxidant functions of AhR is intricately linked to the Nrf2 signaling cascade⁶⁸. Expanding the functional scope of this metabolic cascade, downstream metabolites like cinnabarinic acid further contribute to cellular protection by mitigating OS-induced apoptosis via AhR-dependent mechanisms⁶⁹. In this study, metabolomic profiling revealed a marked elevation in circulating tryptophan catabolites within the LOS group. Given their established roles as potential endogenous antioxidants, endogenous ligands for AhR, and modulators of Nrf2 signaling, these metabolites may critically modulate redox homeostasis in LOS cows. Furthermore, correlation analysis revealed a strong association between tryptophan metabolism and altered hindgut microbial species, including *Azospirillum* sp. 51 20, *unclassified Alphaproteobacteria*, *Ruminococcus* sp. CAG624, *Akkermansia glycaniphila*, *Faecalibacterium prausnitzii*, *Streptomyces* sp. Tu6071, and *Firmicutes bacterium* CAG110 56 8. These findings collectively demonstrate a connection between tryptophan metabolism and an altered hindgut microbiome in OS.

Beyond tryptophan-derived metabolites, microbial SCFAs production emerged as another critical axis linking gut microbiota to redox regulation. Previous studies have established that elevated alpha-diversity reflects a more complex microbial ecosystem, a characteristic linked to enhanced metabolic stability and host antioxidant capacity⁷⁰⁻⁷². Consistent with this, we observed that the LOS group exhibited significantly higher Chao1 and Shannon indices, with these differences correlating with reduced systemic OS. These findings reinforce the protective role of microbial diversity in mitigating redox imbalance via improved ecosystem complexity. Microbial network analysis revealed that the HOS condition significantly disrupted the steady state of the hindgut microbiome in dairy cows. The reduced microbial interactions likely diminished the synergistic effects between bacteria, a phenomenon also observed in calves with underdeveloped gut⁷³. Moreover, within the species-level interaction network, we identified an enrichment of functional bacteria serving as hub nodes in the hindgut of

LOS cows. For example, *Fibrobacteres bacterium* CG2 30 45 31, a typical fiber-degrading bacteria, demonstrated high efficiency in cellulose utilization⁷⁴. Similarly, *Treponema* sp. JC4 and *Treponema bryantii*, identified in the ruminant gastrointestinal tract, ferment soluble sugars derived from cellulose, contributing to fiber degradation and facilitating the generation of SCFAs⁷⁵.

Our fecal metagenomic analysis revealed distinct microbial communities functionally linked to KEGG-annotated SCFA metabolic pathways in LOS and HOS groups⁷⁶. Pyruvate and succinate, which are pivotal fermentation substrates, are likely to serve as key determinants of subsequent SCFAs synthesis. Pyruvate directly contributes to acetate production upon conversion to acetyl CoA, whereas propionate can be generated either via the acrylate route or through the decarboxylation of succinate. Butyrate synthesis arises from the condensation of two acetyl-CoA molecules or utilization of externally sourced acetate⁷⁷. The differential abundance of microbial populations aligned with the notably increased fecal SCFAs concentrations observed in the LOS group, particularly involving key species (*P. succinatutens*, *Bacteroides bacterium*, *Paludibacter propionigenes*, *Clostridium* sp. CAG413, and *unclassified Bacteroidetes*) as significant contributors, exhibiting substantial explained variations in predicting these metabolic pathways. *Bacteroides* spp. and *Clostridium*, for instance, utilize the butyryl-CoA:acetate CoA-transferase pathway, thereby actively contributing to butyrate and acetate production⁷⁸⁻⁸⁰. However, *P. succinatutens* has been implicated in succinate utilization and propionate synthesis. Certain *Clostridium* sp. use the acrylate pathway to synthesize propionate from acryloyl-CoA⁸¹. Building on previous evidence linking host OS to microbial community composition^{82,83}, the observed differences in metabolic pathways were primarily driven by microbial community variations, which directly influence functional metabolic activity and downstream metabolite profiles. In the hindgut, bacteria ferment indigestible carbohydrates into SCFAs, comprising organic acids with one to six carbon atoms⁸⁴. Among these SCFAs, acetate, propionate, and butyrate are the principal components synthesized by the gut microbiota⁸⁵. SCFAs, notably butyrate and propionate, play pivotal roles in modulating host redox homeostasis through multifaceted mechanisms⁴⁸. Recent findings from both human and murine research indicate that gut microbiota dysbiosis accelerates the progression of redox dysregulation in various conditions, including diabetes, neurodegenerative disorders, and cardiovascular diseases⁸⁶⁻⁸⁸, with SCFAs serving as pivotal mediators in this process. Functioning as signaling molecules, SCFAs counteract OS through dual mechanisms: immunomodulatory action via intestinal macrophage polarization toward non-inflammatory phenotypes that enhance bacterial clearance at compromised intestinal barriers^{89,90}, and direct redox regulation through epigenetic and transcriptional modulation. Specifically, SCFAs regulate host redox homeostasis primarily through histone deacetylases (HDACs)-inhibitory epigenetic modulation and promotion of Nrf2 nuclear translocation, exemplified by butyrate's capacity to suppress ROS generation via the cyclin-dependent kinase inhibitor 1 (p21)-Nrf2 signaling in microglia and intestinal epithelia⁹¹, while activating GPR109A-AMPK pathways in bovine epithelial cells⁹². This functional pleiotropy extends to other SCFAs, where acetate preserves pancreatic islets and MIN6 β -cells viability under OS by enhancing metabolic resilience and ROS scavenging⁹³, and propionate activates FFAR3-Nrf2 signaling to protect the blood-brain barrier from OS⁹⁴. Notably, SCFAs act synergistically with omega-3 fatty acids to amplify Nrf2-HO-1 pathway activation, highlighting SCFAs as pivotal mediators linking microbial metabolism to antioxidant defenses⁹⁵. Collectively, these mechanistic insights align with our findings that altered hindgut microbial composition and consequent SCFA levels alteration likely contribute to the development of OS.

Various pathophysiological conditions, including OS, compromise the integrity of the epithelial barrier⁹⁶. Intestinal epithelial tight junction proteins are critical for maintaining mucosal integrity and barrier function through their interactions with the actin cytoskeleton, with key proteins such as claudin-1 and occludin playing vital roles⁹⁷⁻⁹⁹. The Nrf2-Keap1 pathway regulates numerous genes responsive to OS, and *HO-1* acts

downstream of the Nrf2-Keap1 pathway¹⁰⁰. Certain probiotic strains can activate this pathway in the colon, resulting in the enhanced expression of downstream antioxidant enzymes¹⁰¹. SOD serves as a key antioxidant enzyme, catalyzing the dismutation of superoxide radicals, whereas GSH-Px catalyzes the reaction between glutathione and H₂O₂, thereby protecting cellular membranes^{102,103}. Beyond examining the broader effects of OS on gut microbiota and SCFAs metabolism, we focused on identifying the specific microbial species involved in the development of OS. Notably, we found that a low OS increased the abundance of *P. succinatutens*, a species associated with beta-alanine, butanoate, propanoate, and pyruvate metabolism. *P. succinatutens*, a succinate-utilizing bacterium known to produce propionate, has demonstrated potential to compete with *Clostridioides difficile*, mitigate dysbiosis, and restore microbial balance. This highlights the potential therapeutic applications targeting *Clostridioides difficile* infections⁵⁷. Interestingly, previous studies have linked decreased fecal abundance of *P. succinatutens* to increased OS in both the host and gut^{55,56}. However, their specific antioxidant capacity remains largely unexplored. Thus, we conducted a validation study in mice to confirm the antioxidant effects of *P. succinatutens* on both the host and the colon. In this study, oral gavage of *P. succinatutens* significantly enhanced the systemic antioxidant capacity, as evidenced by increased serum TAOC and decreased levels of TOS and OSI. Mice receiving this probiotic exhibited improved colonic integrity with significantly elevated expression of *claudin-1* and *occludin* in the colon tissue. Furthermore, treatment with *P. succinatutens* upregulated genes associated with the Nrf2-Keap1 antioxidant pathway, increased the colonic expression of *Nrf2* and *HO-1*, and enhanced the activities of GSH-Px and SOD while simultaneously downregulating the expression of colonic *Keap1*. The observed increase in propionate following *P. succinatutens* treatment in the TRT group likely stems from its unique metabolic activity, as this bacteria mainly utilizes succinate as a substrate to enhance propionate production¹⁰⁴. Notably, previous studies demonstrated that acetate and propionate play critical roles in maintaining blood-brain barrier (BBB) integrity by reducing permeability and upregulating tight junction protein expression. Furthermore, propionate has been shown to activate the Nrf2 signaling pathway, effectively scavenging ROS and protecting the BBB against OS⁹⁴. In our study, these mechanisms align with the findings that elevated acetate and propionate levels contribute to enhanced epithelial barrier function and Nrf2-mediated antioxidant responses. Furthermore, our data revealed a significant upregulation of colonic antioxidant enzyme expression in response to *P. succinatutens* intervention, suggesting the intestinal tract as a direct target of its activity. Collectively, these results suggest that specific SCFAs produced by *P. succinatutens*, particularly propionate, may promote redox homeostasis through Nrf2-Keap1 pathway activation, thereby elucidating a molecular mechanism underlying probiotic-mediated antioxidant defense.

Overall, we identified tryptophan metabolism and an imbalance in SCFAs production as concurrent determinants of the hindgut microbiota in contributing to OS. Our findings suggest that targeting hindgut microbiota and microbial metabolites may offer a promising strategy for novel therapeutic interventions aimed at alleviating OS. Furthermore, using a murine model, we provide valuable insights into probiotic-mediated host and colonic antioxidant responses, positioning *P. succinatutens* as a compelling candidate for probiotic development in the future.

Data availability

The 16S rRNA gene sequencing and metagenomics data in this study were submitted to the SRA database in NCBI: # PRJNA1171342.

Received: 10 December 2024; Accepted: 7 April 2025;

Published online: 22 April 2025

References

- Bhattacharyya, A., Chattopadhyay, R., Mitra, S. & Crowe, S. E. Oxidative stress: an essential factor in the pathogenesis of gastrointestinal mucosal diseases. *Physiol. Rev.* **94**, 329–354 (2014).
- Darenskaya, M. A., Kolesnikova, L. I. & Kolesnikov, S. I. Oxidative stress: pathogenetic role in diabetes mellitus and its complications and therapeutic approaches to correction. *Bull. Exp. Biol. Med.* **171**, 179–189 (2021).
- Forman, H. J. & Zhang, H. Targeting oxidative stress in disease: promise and limitations of antioxidant therapy. *Nat. Rev. Drug Discov.* **20**, 689–709 (2021).
- Jadeja, R. N., Devkar, R. V. & Nammi, S. Oxidative stress in liver diseases: pathogenesis, prevention, and therapeutics. *Oxid. Med. Cell Longev.* **2017**, 8341286 (2017).
- Abuelo, A., Hernández, J., Benedito, J. L. & Castillo, C. The importance of the oxidative status of dairy cattle in the periparturient period: revisiting antioxidant supplementation. *J. Anim. Physiol. Anim. Nutr.* **99**, 1003–1016 (2015).
- Kim, J. H., Moon, N., Heo, S. J., Jeong, Y. W. & Kang, D. R. Repeated measurements and mixture effects of urinary bisphenols, parabens, polycyclic aromatic hydrocarbons, and other chemicals on biomarkers of oxidative stress in pre- and postpartum women. *Environ. Pollut.* **342**, 123057 (2024).
- Li, Q., Yang, S., Chen, F., Guan, W. & Zhang, S. Nutritional strategies to alleviate oxidative stress in sows. *Anim. Nutr.* **9**, 60–73 (2022).
- Roca-Rodríguez, M. M. et al. Postpartum development of endothelial dysfunction and oxidative stress markers in women with previous gestational diabetes mellitus. *J. Endocrinol. Investig.* **37**, 503–509 (2014).
- Carvalho, M. R. et al. Long-term effects of postpartum clinical disease on milk production, reproduction, and culling of dairy cows. *J. Dairy Sci.* **102**, 11701–11717 (2019).
- McGuffey, R. K. A 100-year review: metabolic modifiers in dairy cattle nutrition. *J. Dairy Sci.* **100**, 10113–10142 (2017).
- Tempelman, R. J. & Lu, Y. Symposium review: genetic relationships between different measures of feed efficiency and the implications for dairy cattle selection indexes. *J. Dairy Sci.* **103**, 5327–5345 (2020).
- Bell, A. W. Regulation of organic nutrient metabolism during transition from late pregnancy to early lactation. *J. Anim. Sci.* **73**, 2804–2819 (1995).
- Castillo, C. et al. Oxidative status during late pregnancy and early lactation in dairy cows. *Vet. J.* **169**, 286–292 (2005).
- Sordillo, L. M. & Aitken, S. L. Impact of oxidative stress on the health and immune function of dairy cattle. *Vet. Immunol. Immunopathol.* **128**, 104–109 (2009).
- Hummel, G. L., Austin, K. & Cunningham-Hollinger, H. C. Comparing the maternal-fetal microbiome of humans and cattle: a translational assessment of the reproductive, placental, and fetal gut microbiomes. *Biol. Reprod.* **107**, 371–381 (2022).
- Sies, H. & Cadenas, E. Oxidative stress: damage to intact cells and organs. *Philos. Trans. R. Soc. Lond. B Biol. Sci.* **311**, 617–631 (1985).
- Abuelo, A., Hernández, J., Benedito, J. L. & Castillo, C. Oxidative stress index (OSI) as a new tool to assess redox status in dairy cattle during the transition period. *Animal* **7**, 1374–1378 (2013).
- Sharma, R. K., Pasqualotto, F. F., Nelson, D. R., Thomas, A. J. Jr & Agarwal, A. The reactive oxygen species-total antioxidant capacity score is a new measure of oxidative stress to predict male infertility. *Hum. Reprod.* **14**, 2801–2807 (1999).
- Qiao, Y., Sun, J., Ding, Y., Le, G. & Shi, Y. Alterations of the gut microbiota in high-fat diet mice is strongly linked to oxidative stress. *Appl. Microbiol. Biotechnol.* **97**, 1689–1697 (2013).
- Li, T. et al. Tempol ameliorates polycystic ovary syndrome through attenuating intestinal oxidative stress and modulating of gut microbiota composition-serum metabolites interaction. *Redox Biol.* **41**, 101886 (2021).
- Uchiyama, J., Akiyama, M., Hase, K., Kumagai, Y. & Kim, Y. G. Gut microbiota reinforce host antioxidant capacity via the generation of reactive sulfur species. *Cell Rep.* **38**, 110479 (2022).

22. Gyuraszova, M., Kovalcikova, A. & Gardlik, R. Association between oxidative status and the composition of intestinal microbiota along the gastrointestinal tract. *Med. Hypotheses* **103**, 81–85 (2017).
23. Chen, F. et al. Integrated analysis of the faecal metagenome and serum metabolome reveals the role of gut microbiome-associated metabolites in the detection of colorectal cancer and adenoma. *Gut* **71**, 1315–1325 (2022).
24. Krautkramer, K. A., Fan, J. & Bäckhed, F. Gut microbial metabolites as multi-kingdom intermediates. *Nat. Rev. Microbiol.* **19**, 77–94 (2021).
25. Liu, R. et al. Gut microbiome and serum metabolome alterations in obesity and after weight-loss intervention. *Nat. Med.* **23**, 859–868 (2017).
26. Banwo, K., Alonge, Z. & Sanni, A. I. Binding capacities and antioxidant activities of *Lactobacillus plantarum* and *Pichia kudriavzevii* against cadmium and lead toxicities. *Biol. Trace Elem. Res.* **199**, 779–791 (2021).
27. Zamani, B., Sheikhi, A., Namazi, N., Larijani, B. & Azadbakht, L. The effects of supplementation with probiotic on biomarkers of oxidative stress in adult subjects: a systematic review and meta-analysis of randomized trials. *Probiot. Antimicrob. Proteins* **12**, 102–111 (2020).
28. Pinedo, P. J., Manríquez, D., Ciarletta, C., Azocar, J., De Vries, A. Association between body condition score fluctuations and pregnancy loss in Holstein cows. *J. Anim. Sci.* **100**, skac266 (2022).
29. Gu, F. et al. Gut microbiome is linked to functions of peripheral immune cells in transition cows during excessive lipolysis. *Microbiome* **11**, 40 (2023).
30. Caporaso, J. G. et al. QIIME allows analysis of high-throughput community sequencing data. *Nat. Methods* **7**, 335–336 (2010).
31. Zhang, J., Kobert, K., Flouri, T. & Stamatakis, A. PEAR: a fast and accurate Illumina Paired-End reAd mergeR. *Bioinformatics* **30**, 614–620 (2014).
32. Rognes, T., Flouri, T., Nichols, B., Quince, C. & Mahé, F. VSEARCH: a versatile open source tool for metagenomics. *PeerJ* **4**, e2584 (2016).
33. Edgar, R. C., Haas, B. J., Clemente, J. C., Quince, C. & Knight, R. UCHIME improves sensitivity and speed of chimera detection. *Bioinformatics* **27**, 2194–2200 (2011).
34. Edgar, R. C. UPARSE: highly accurate OTU sequences from microbial amplicon reads. *Nat. Methods* **10**, 996–998 (2013).
35. Pruesse, E. et al. SILVA: a comprehensive online resource for quality checked and aligned ribosomal RNA sequence data compatible with ARB. *Nucleic Acids Res.* **35**, 7188–7196 (2007).
36. Ye, J., McGinnis, S. & Madden, T. L. BLAST: improvements for better sequence analysis. *Nucleic Acids Res.* **34**, W6–W9 (2006).
37. Chen, S., Zhou, Y., Chen, Y. & Gu, J. fastp: an ultra-fast all-in-one FASTQ preprocessor. *Bioinformatics* **34**, i884–i890 (2018).
38. Langmead, B. & Salzberg, S. L. Fast gapped-read alignment with Bowtie 2. *Nat. Methods* **9**, 357–359 (2012).
39. Buchfink, B., Xie, C. & Huson, D. H. Fast and sensitive protein alignment using DIAMOND. *Nat. Methods* **12**, 59–60 (2015).
40. Shi, Y. et al. Interannual climate variability and altered precipitation influence the soil microbial community structure in a Tibetan Plateau grassland. *Sci. Total Environ.* **714**, 136794 (2020).
41. Dunn, W. B. et al. Procedures for large-scale metabolic profiling of serum and plasma using gas chromatography and liquid chromatography coupled to mass spectrometry. *Nat. Protoc.* **6**, 1060–1083 (2011).
42. Zhou, B., Xiao, J. F., Tuli, L. & Ransom, H. W. LC-MS-based metabolomics. *Mol. Biosyst.* **8**, 470–481 (2012).
43. Chong, J. & Xia, J. MetaboAnalystR: an R package for flexible and reproducible analysis of metabolomics data. *Bioinformatics* **34**, 4313–4314 (2018).
44. Boccard, J. & Rutledge, D. N. A consensus orthogonal partial least squares discriminant analysis (OPLS-DA) strategy for multiblock Omics data fusion. *Anal. Chim. Acta* **769**, 30–39 (2013).
45. Hoyles, L. et al. Molecular phenomics and metagenomics of hepatic steatosis in non-diabetic obese women. *Nat. Med.* **24**, 1070–1080 (2018).
46. Ni, Y. et al. Resistant starch decreases intrahepatic triglycerides in patients with NAFLD via gut microbiome alterations. *Cell Metab.* **35**, 1530–1547.e1538 (2023).
47. Gasmi, A. et al. An update on glutathione's biosynthesis, metabolism, functions, and medicinal purposes. *Curr. Med. Chem.* **31**, 4579–4601 (2024).
48. González-Bosch, C., Boorman, E., Zunszain, P. A. & Mann, G. E. Short-chain fatty acids as modulators of redox signaling in health and disease. *Redox Biol.* **47**, 102165 (2021).
49. Goossens, J. F. & Bailly, C. Ursodeoxycholic acid and cancer: From chemoprevention to chemotherapy. *Pharm. Ther.* **203**, 107396 (2019).
50. Ji, Y., Gao, Y., Chen, H., Yin, Y., Zhang, W. Indole-3-acetic acid alleviates nonalcoholic fatty liver disease in mice via attenuation of hepatic lipogenesis, and oxidative and inflammatory stress. *Nutrients* **11**, 2062 (2019).
51. Martínez, Y. et al. The role of methionine on metabolism, oxidative stress, and diseases. *Amino Acids* **49**, 2091–2098 (2017).
52. Vojinovic, D. et al. Relationship between gut microbiota and circulating metabolites in population-based cohorts. *Nat. Commun.* **10**, 5813 (2019).
53. Zhang, B. et al. Characteristics of serum metabolites and gut microbiota in diabetic kidney disease. *Front Pharm.* **13**, 872988 (2022).
54. Zhou, K. et al. Integrated macrogenomics and metabolomics explore alterations and correlation between gut microbiota and serum metabolites in adult epileptic patients: a pilot study. *Microorganisms* **11**, 2628 (2023).
55. Cai, L. et al. The effects of dietary silybin supplementation on the growth performance and regulation of intestinal oxidative injury and microflora dysbiosis in weaned piglets. *Antioxidants* **12**, 1975 (2023).
56. Duarte, M. E., Stahl, C. H. & Kim, S. W. Intestinal damages by F18⁺ *Escherichia coli* and its amelioration with an antibacterial bacitracin fed to nursery pigs. *Antioxidants* **12**, 1040 (2023).
57. Nagao-Kitamoto, H. et al. Interleukin-22-mediated host glycosylation prevents *Clostridioides difficile* infection by modulating the metabolic activity of the gut microbiota. *Nat. Med.* **26**, 608–617 (2020).
58. Ye, D. et al. Integrative metagenomic and metabolomic analyses reveal gut microbiota-derived multiple hits connected to development of gestational diabetes mellitus in humans. *Gut Microbes* **15**, 2154552 (2023).
59. Anderson, G. & Maes, M. Bipolar disorder: role of immune-inflammatory cytokines, oxidative and nitrosative stress and tryptophan catabolites. *Curr. Psychiatry Rep.* **17**, 8 (2015).
60. Yin, J. et al. Ameliorative effect of dietary tryptophan on neurodegeneration and inflammation in D-Galactose-induced aging mice with the potential mechanism relying on AMPK/SIRT1/PGC-1α Pathway and gut microbiota. *J. Agric. Food Chem.* **69**, 4732–4744 (2021).
61. Didara, M. et al. Immune and oxidative response to linseed in the diet of periparturient Holstein cows. *Animal* **9**, 1349–1354 (2015).
62. Bühler, S. et al. Effects of energy supply and nicotinic acid supplementation on serum anti-oxidative capacity and on expression of oxidative stress-related genes in blood leucocytes of periparturient primi- and pluriparous dairy cows. *J. Anim. Physiol. Anim. Nutr.* **102**, e87–e98 (2018).
63. Wullepit, N. et al. Influence of a marine algae supplementation on the oxidative status of plasma in dairy cows during the periparturient period. *Prev. Vet. Med.* **103**, 298–303 (2012).
64. Ramírez Ortega, D. et al. On the antioxidant properties of L-kynurenine: an efficient ROS scavenger and enhancer of rat brain antioxidant defense. *Antioxidants* **11**, 31 (2021).

65. Reyes Ocampo, J. et al. Kynurenines with neuroactive and redox properties: relevance to aging and brain diseases. *Oxid. Med. Cell Longev.* **2014**, 646909 (2014).
66. Genestet, C. et al. Scavenging of reactive oxygen species by tryptophan metabolites helps *Pseudomonas aeruginosa* escape neutrophil killing. *Free Radic. Biol. Med.* **73**, 400–410 (2014).
67. Kaiser, H., Parker, E. & Hamrick, M. W. Kynurenine signaling through the aryl hydrocarbon receptor: Implications for aging and healthspan. *Exp. Gerontol.* **130**, 110797 (2020).
68. Xu, K., Liu, G. & Fu, C. The tryptophan pathway targeting antioxidant capacity in the placenta. *Oxid. Med. Cell Longev.* **2018**, 1054797 (2018).
69. Joshi, A. D., Carter, D. E., Harper, T. A. Jr & Elferink, C. J. Aryl hydrocarbon receptor-dependent stanniocalcin 2 induction by cinnabarinic acid provides cytoprotection against endoplasmic reticulum and oxidative stress. *J. Pharm. Exp. Ther.* **353**, 201–212 (2015).
70. Bello-Corral, L. et al. Implications of gut and oral microbiota in neuroinflammatory responses in Alzheimer's disease. *Life Sci.* **333**, 122132 (2023).
71. Larsen, O. F. A. & Claassen, E. The mechanistic link between health and gut microbiota diversity. *Sci. Rep.* **8**, 2183 (2018).
72. Segata, N. Gut microbiome: westernization and the disappearance of intestinal diversity. *Curr. Biol.* **25**, R611–R613 (2015).
73. Zhuang, Y. et al. The Bifidobacterium-dominated fecal microbiome in dairy calves shapes the characteristic growth phenotype of host. *NPJ Biofilms Microbiomes* **10**, 59 (2024).
74. Fakih, I. et al. Dynamic genome-based metabolic modeling of the predominant cellulolytic rumen bacterium *Fibrobacter succinogenes* S85. *mSystems* **8**, e0102722 (2023).
75. Rosewarne, C. P. et al. Draft genome sequence of *Treponema* sp. strain JC4, a novel spirochete isolated from the bovine rumen. *J. Bacteriol.* **194**, 4130 (2012).
76. Koh, A., De Vadder, F., Kovatcheva-Datchary, P. & Bäckhed, F. From dietary fiber to host physiology: short-chain fatty acids as key bacterial metabolites. *Cell* **165**, 1332–1345 (2016).
77. den Besten, G. et al. The role of short-chain fatty acids in the interplay between diet, gut microbiota, and host energy metabolism. *J. Lipid Res.* **54**, 2325–2340 (2013).
78. Flint, H. J., Duncan, S. H., Scott, K. P. & Louis, P. Links between diet, gut microbiota composition and gut metabolism. *Proc. Nutr. Soc.* **74**, 13–22 (2015).
79. Louis, P., Young, P., Holtrop, G. & Flint, H. J. Diversity of human colonic butyrate-producing bacteria revealed by analysis of the butyryl-CoA:acetate CoA-transferase gene. *Environ. Microbiol.* **12**, 304–314 (2010).
80. Reichardt, N. et al. Phylogenetic distribution of three pathways for propionate production within the human gut microbiota. *Isme J.* **8**, 1323–1335 (2014).
81. Hetzel, M. et al. Acryloyl-CoA reductase from *Clostridium propionicum*. An enzyme complex of propionyl-CoA dehydrogenase and electron-transferring flavoprotein. *Eur. J. Biochem.* **270**, 902–910 (2003).
82. Kunst, C. et al. The influence of gut microbiota on oxidative stress and the immune system. *Biomedicines*. **11**, 1388 (2023).
83. Mostafavi Abdolmaleky, H., Zhou, J. R. Gut microbiota dysbiosis, oxidative stress, inflammation, and epigenetic alterations in metabolic diseases. *Antioxidants*. **13**, 985 (2024).
84. David, L. A. et al. Diet rapidly and reproducibly alters the human gut microbiome. *Nature* **505**, 559–563 (2014).
85. Miller, T. L. & Wolin, M. J. Pathways of acetate, propionate, and butyrate formation by the human fecal microbial flora. *Appl. Environ. Microbiol.* **62**, 1589–1592 (1996).
86. Battson, M. L., Lee, D. M., Weir, T. L. & Gentile, C. L. The gut microbiota as a novel regulator of cardiovascular function and disease. *J. Nutr. Biochem.* **56**, 1–15 (2018).
87. Long-Smith, C. et al. Microbiota-gut-brain axis: new therapeutic opportunities. *Annu. Rev. Pharm. Toxicol.* **60**, 477–502 (2020).
88. Moreno-Indias, I., Cardona, F., Tinahones, F. J. & Queipo-Ortuño, M. I. Impact of the gut microbiota on the development of obesity and type 2 diabetes mellitus. *Front. Microbiol.* **5**, 190 (2014).
89. Hamer, H. M. et al. Review article: the role of butyrate on colonic function. *Aliment Pharm. Ther.* **27**, 104–119 (2008).
90. Sun, M., Wu, W., Liu, Z. & Cong, Y. Microbiota metabolite short chain fatty acids, GPCR, and inflammatory bowel diseases. *J. Gastroenterol.* **52**, 1–8 (2017).
91. Kim, S. Y. et al. Sodium butyrate inhibits high cholesterol-induced neuronal amyloidogenesis by modulating NRF2 stabilization-mediated ROS levels: involvement of NOX2 and SOD1. *Cell Death Dis.* **11**, 469 (2020).
92. Guo, W., et al. Butyrate alleviates oxidative stress by regulating NRF2 nuclear accumulation and H3K9/14 acetylation via GPR109A in bovine mammary epithelial cells and mammary glands. *Free Radic. Biol. Med.* **152**, 728–742 (2020).
93. Hu, S., Kuwabara, R., de Haan, B. J., Smink, A. M., de Vos, P. Acetate and butyrate improve β -cell metabolism and mitochondrial respiration under oxidative stress. *Int. J. Mol. Sci.* **21**, 1542 (2020).
94. Hoyles, L. et al. Microbiome-host systems interactions: protective effects of propionate upon the blood-brain barrier. *Microbiome* **6**, 55 (2018).
95. Geng, X. et al. Effects of docosahexaenoic acid and its peroxidation product on amyloid- β peptide-stimulated microglia. *Mol. Neurobiol.* **57**, 1085–1098 (2020).
96. Gareau, M. G., Silva, M. A. & Perdue, M. H. Pathophysiological mechanisms of stress-induced intestinal damage. *Curr. Mol. Med.* **8**, 274–281 (2008).
97. Feldman, G. J., Mullin, J. M. & Ryan, M. P. Occludin: structure, function and regulation. *Adv. Drug Deliv. Rev.* **57**, 883–917 (2005).
98. Furuse, M. et al. Claudin-based tight junctions are crucial for the mammalian epidermal barrier: a lesson from claudin-1-deficient mice. *J. Cell Biol.* **156**, 1099–1111 (2002).
99. González-Mariscal, L., Betanzos, A., Nava, P. & Jaramillo, B. E. Tight junction proteins. *Prog. Biophys. Mol. Biol.* **81**, 1–44 (2003).
100. Bellezza, I., Giambanco, I., Minelli, A. & Donato, R. Nrf2-Keap1 signaling in oxidative and reductive stress. *Biochim. Biophys. Acta Mol. Cell Res.* **1865**, 721–733 (2018).
101. Gao, Y. et al. *Lactobacillus plantarum* Y44 alleviates oxidative stress by regulating gut microbiota and colonic barrier function in Balb/C mice with subcutaneous D-galactose injection. *Food Funct.* **12**, 373–386 (2021).
102. Balendra, V. & Singh, S. K. Therapeutic potential of astaxanthin and superoxide dismutase in Alzheimer's disease. *Open Biol.* **11**, 210013 (2021).
103. Flohé, L., Toppo, S. & Orian, L. The glutathione peroxidase family: discoveries and mechanism. *Free Radic. Biol. Med.* **187**, 113–122 (2022).
104. Watanabe, Y., Nagai, F. & Morotomi, M. Characterization of *Phascolarctobacterium succinatutens* sp. nov., an asaccharolytic, succinate-utilizing bacterium isolated from human feces. *Appl. Environ. Microbiol.* **78**, 511–518 (2012).

Acknowledgements

We thank Mei Ma, Jiaying Ma, Shuangyi Wang, Xiaotong Kang, and Tianhao Dong from China Agricultural University (Beijing, P. R. China) for their kind help during this study. This work was supported by the Key Research and Development Program of Ningxia (2024BBF01006), the National Key Research and Development Program of China (2023YFD1300904), the National Center of Technology Innovation for Dairy (2024-KFKT-026) and the Pinduoduo-China Agricultural University Research Fund (PC2023B02002). We also thank Gang Guo and Kebi Hao (Beijing Sunlon Livestock Development Co., Ltd.) for their support during the farm trial.

Author contributions

Z.C. served as principal investigator and provided financial support. S.L., W.W., and M.L. designed the experiment. B.M., Y.Z., Y.X., H.Z., Y.N., G.H., and J.X. conducted the experiment. D.G., Y.Z., B.M., T.C., G.H., W.G., J.Y., and Z.H. collected samples. D.G., Y.Z., and S.L. analysed data. D.G. wrote the manuscript. S.L. and Y.Z. revised the manuscript.

Competing interests

The authors declare no competing interests.

Ethics approval

The animal care protocol received approval from the Animal Care and Use Committee of China Agricultural University (Protocol Number: AW10803202-3-1) and the Beijing Laboratory Animal Research Center (Protocol Number: BLARC-LAWER-202404003).

Additional information

Supplementary information The online version contains supplementary material available at <https://doi.org/10.1038/s41522-025-00698-7>.

Correspondence and requests for materials should be addressed to Zhijun Cao.

Reprints and permissions information is available at <http://www.nature.com/reprints>

Publisher's note Springer Nature remains neutral with regard to jurisdictional claims in published maps and institutional affiliations.

Open Access This article is licensed under a Creative Commons Attribution-NonCommercial-NoDerivatives 4.0 International License, which permits any non-commercial use, sharing, distribution and reproduction in any medium or format, as long as you give appropriate credit to the original author(s) and the source, provide a link to the Creative Commons licence, and indicate if you modified the licensed material. You do not have permission under this licence to share adapted material derived from this article or parts of it. The images or other third party material in this article are included in the article's Creative Commons licence, unless indicated otherwise in a credit line to the material. If material is not included in the article's Creative Commons licence and your intended use is not permitted by statutory regulation or exceeds the permitted use, you will need to obtain permission directly from the copyright holder. To view a copy of this licence, visit <http://creativecommons.org/licenses/by-nc-nd/4.0/>.

© The Author(s) 2025